

The British University in Egypt

**BUE Scholar**

---

Pharmacy

Health Sciences

---

Winter 2-10-2023

## Challenging breast cancer through novel sulfonamide–pyridine hybrids: design, synthesis, carbonic anhydrase IX inhibition and induction of apoptosis.

Amira Khalil

*Department of Pharmaceutical Chemistry, Faculty of Pharmacy, The British University in Egypt (BUE), El-Sherouk City, Cairo, 11837, Egypt., amira.khalil@bue.edu.eg*

Nashwa H. Zaher

*Drug Radiation Research, National Center for Radiation Research & Technology (NCRRT), Egyptian Atomic Energy Authority, Cairo, Egypt*

Reham MM Elhazek

*Drug Radiation Research, National Center for Radiation Research & Technology (NCRRT), Egyptian Atomic Energy Authority, Cairo, Egypt*

Ahmed E. Gouda

*Pharmaceutical Research Department, Nawah Scientific, Cairo, Egypt*

Marwa G. Elgazzar

*Drug Radiation Research, National Center for Radiation Research & Technology (NCRRT), Egyptian Atomic Energy Authority, Cairo, Egypt*

 Part of the [Chemicals and Drugs Commons](#), [Diseases Commons](#), and the [Medicinal and Pharmaceutical Chemistry Commons](#)

---

### Recommended Citation

Khalil, Amira; Zaher, Nashwa H.; Elhazek, Reham MM; Gouda, Ahmed E.; and Elgazzar, Marwa G., "Challenging breast cancer through novel sulfonamide–pyridine hybrids: design, synthesis, carbonic anhydrase IX inhibition and induction of apoptosis." (2023). *Pharmacy*. 607.  
<https://buescholar.bue.edu.eg/pharmacy/607>

This Article is brought to you for free and open access by the Health Sciences at BUE Scholar. It has been accepted for inclusion in Pharmacy by an authorized administrator of BUE Scholar. For more information, please contact [bue.scholar@gmail.com](mailto:bue.scholar@gmail.com).

For reprint orders, please contact: [reprints@future-science.com](mailto:reprints@future-science.com)

# Challenging breast cancer through novel sulfonamide–pyridine hybrids: design, synthesis, carbonic anhydrase IX inhibition and induction of apoptosis

Nashwa H Zaher<sup>1</sup> , Reham MM Elhazek<sup>1</sup>, Ahmed E Gouda<sup>2</sup>, Amira Khalil<sup>\*,3,4</sup> & Marwa G Elgazzar<sup>1</sup>

<sup>1</sup>Drug Radiation Research, National Center for Radiation Research & Technology (NCRRT), Egyptian Atomic Energy Authority, Cairo, Egypt

<sup>2</sup>Pharmaceutical Research Department, Nawah Scientific, Cairo, Egypt

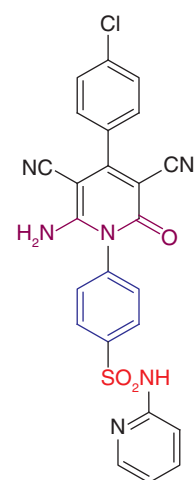
<sup>3</sup>Department of Pharmaceutical Chemistry, Faculty of Pharmacy, The British University in Egypt (BUE), El-Sherouk City, Cairo, 11837, Egypt

<sup>4</sup>The Center for Drug Research & Development (CDRD), Faculty of Pharmacy, The British University in Egypt (BUE), El-Sherouk City, Cairo, 11837, Egypt

\*Author for correspondence: [Amira.Khalil@bue.edu.eg](mailto:Amira.Khalil@bue.edu.eg)

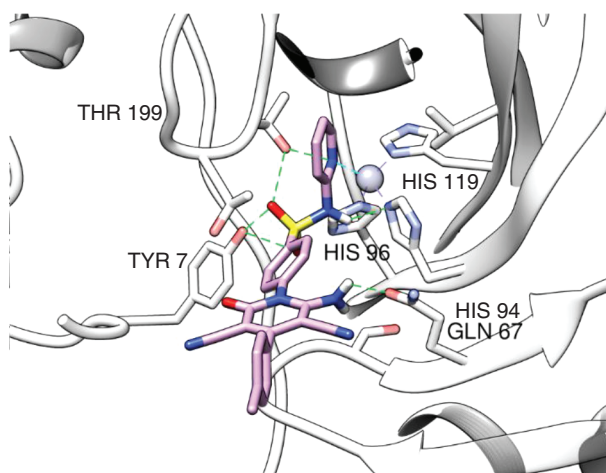
**Background:** Among the important key modulators of the tumor microenvironment and hypoxia is a family of enzymes named carbonic anhydrases. Herein, 11 novel sulfonamide–pyridine hybrids (**2–12**) were designed, synthesized and biologically evaluated for their potential use in targeting breast cancer. **Methods & results:** The para chloro derivative **7** reported the highest cytotoxic activity against the three breast cancer cell lines used. In addition, compound **7** was found to induce cell cycle arrest and autophagy as well as delaying wound healing. The  $IC_{50}$  of compound **7** against carbonic anhydrase IX was  $253 \pm 12$  nM using dorzolamide HCl as control. **Conclusion:** This study encourages us to expand the designed library, where more sulfonamide derivatives would be synthesized and studied for their structure–activity relationships.

## Graphical abstract:



Compound 7

$IC_{50}$  CA IX =  $253 \pm 12$  nm



First draft submitted: 13 August 2022; Accepted for publication: 1 December 2022; Published online: 10 February 2023

**Keywords:** apoptosis • breast cancer • carbonic anhydrase • hypoxia • sulfonamides

newlands  
press

Cancer presents a serious global health burden which is increasing with growth in population, inappropriate life habits and aging. Cancer is defined as a group of diseases characterized by fast, uncontrolled and pathological cellular division [1]. In 2018, WHO reported almost 9.6 million deaths due to cancer [2]. Despite the presence of hundreds of anticancer agents to date approved by the US FDA, a huge effort still needs to be made in exploring novel anticancer agents [3]. This is mainly to overcome the rapid emergence of drug resistance as well as the many unwanted off-target side effects [4]. Medicinal chemists are in a continuous search for new, more efficient, anticancer agents with minimal side effects. This is usually accomplished by the discovery of novel cancer targets [5]. Nowadays, many researchers are trying to better understand the tumor microenvironment, which plays a significant role in tumorigenesis [6]. The tumor microenvironment is composed of multiple factors which form this complicated network; nutrients, oxygen level, metabolites, pH and growth factors are among these factors [7].

Hypoxia happens when the oxygen supply to tumor cells is not sufficient to their growth needs, and it plays a critical role in the tumor microenvironment [8]. Especially in solid tumors, hypoxia triggers many cellular responses, which include decreased cellular adhesion, proliferation, elevated levels of cellular migration and invasiveness as well as increased angiogenesis [9,10]. All these responses will make the tumor more robust and resistant to the available chemo-, radio- and immunotherapies [11]. On the molecular level, these responses result in remarkable alterations in the transcriptome and proteome of the hypoxic cells [12,13]. These changes are mainly managed by a transcriptional factor called hypoxia-inducible factor (HIF) [14] which greatly affects tumor proliferation, survival and metastasis [15] through the overexpression of certain genes and proteins. Among the genes which are the target for HIF's actions are those mediating angiogenesis (e.g., *VEGF* and *VEGFR*), glycolytic pathway enzymes (e.g. *LDH*, *HK2*) and glucose transporters (*GLUT1*, *GLUT3*) [9,16]. Herein, we will focus on one of the enzymes which is greatly affected by hypoxic conditions and HIF, which is carbonic anhydrase IX (CA IX).

CA IX is a member of the  $\alpha$ -carbonic anhydrase family, which includes another 15 human isoforms [17]. This family of enzymes contributes to almost all the physiological steps that involve transport of water and ions as well as pH homeostasis [18]. Carbonic anhydrases are metalloenzymes which are widely distributed in different cellular compartments and act on carbon dioxide, converting it into protons and bicarbonate ions. All CA isoforms except CA IX are present in the normal cells of differentiated tissues; CA XII is present in breast and kidney cancers, and CA II in brain tumors [19–21]. Given that CA IX expression is cancer-associated, it could be considered a potential target for the discovery of novel anticancer agents. Furthermore, it has been discovered that depletion or inhibition of CA IX activity could play a role in breast cancer tumor growth inhibition as well as metastasis [22]. In females, breast cancer is the most common malignancy, with more than 1 million newly diagnosed cancer cases and 502,000 breast cancer-related deaths per year [23]. Breast cancer tissue is made up of various cell types which express a variety of cell surface markers, with altered growth rates and microscopic appearances [24].

Apoptosis and autophagy are two essential mechanisms for maintaining proper cell functions and housekeeping [25]. Cancer cells are well known to escape apoptosis, a programmed cell death that is essential for normal cellular functions [26]. Suppression of apoptosis by cancer cells results in treatment resistance, which motivates researchers to develop new agents with apoptosis-inducing abilities. Several factors affect autophagy, including organelle damage, lack of nutrients and the accumulation of abnormal proteins [27,28]. In addition, hypoxia plays an essential role in autophagy regulation, resulting in lowering the cellular oxidative stress [29]. In cancer research, it has been discovered that autophagy can promote both tumor proliferation and tumor suppression [30]. Various anticancer agents play a role in autophagy regulation and hence could contribute to cellular death or survival [31].

Our research team was inspired by lots of work already done in the area of drug discovery of novel agents targeting cancer using a sulfonamide scaffold [32–43]. Since 2005, sulfonamides have attracted great attention for their carbonic anhydrase inhibition and hence their potential use as anticancer agents [44–46]. Most effort has been made toward the discovery of small molecules targeting CA IX and XII, which are cancer related [47,48]. Many of the discovered molecules showed potential inhibition toward CA IX and/or XII, with very good selectivity over the other isoforms. Many of these molecules share primary sulfonamide or sulfamate groups, as shown in Figure 1A & B [49,50]. Furthermore, it has been reported that SLC-0111, a ureido-substituted benzene sulfonamide molecule, exhibited great promise in phase Ib/II clinical trials [51,52].

Despite the presence of many anticancer agents, there is still a huge need for the development of new anticancer agents with targeted mechanisms, fewer side effects and the ability to fight the emerging drug resistance [53]. The main current treatment for breast cancer is doxorubicin, but unfortunately there is high drug resistance

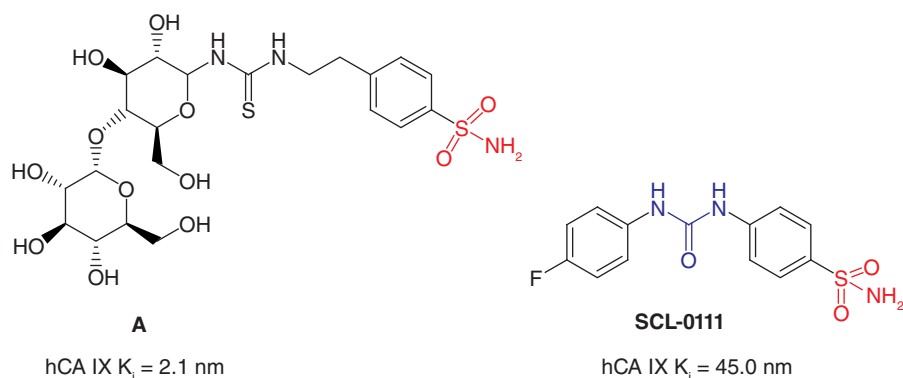


Figure 1. Examples of sulfonamide-based molecules with their  $K_i$  values toward CA XI.

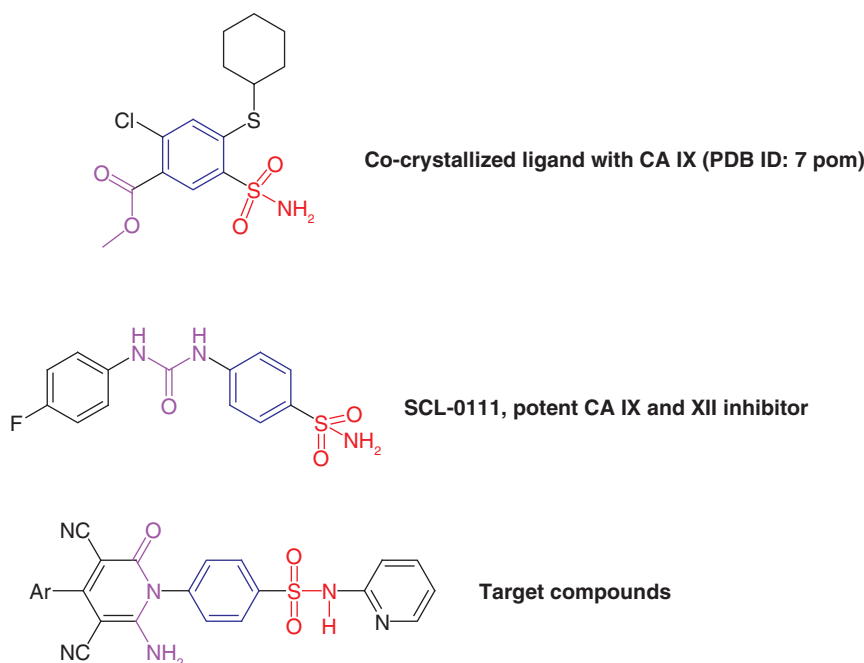


Figure 2. Design of sulfonamide–pyrimidine hybrids as the target library.

associated with its use [54]. Herein we investigated the use of novel synthesized pyridine–sulfonamide hybrids as potential therapeutic agents for breast cancer. In the current work, we decided to apply a molecular hybridization concept [55] for designing our target library. Figure 2 shows the structure of our target compounds; the design process involved molecular hybridization between sulfonamides and pyridine scaffolds with the aim to produce more potent molecules with a wider spectrum of targets. The pyridine nucleus has been already widely studied and evaluated for its diverse pharmacological effects, with special interest in its anticancer activity [56–59]. The design of our target compounds was led by the structural similarities between the co-crystallized ligand (Protein Data Bank [PDB] ID: 7POM) as well as a potent CA IX and CA XII inhibitor, SLC-0111, as shown in Figure 2.

Herein we report the design, synthesis and molecular modeling studies of our target compounds. The synthesized target compounds were tested for their activity against breast cancer. The most potent compound, 7, was used for further studies including apoptosis, autophagy and cell cycle analysis as well as wound healing assessment. Finally, CA IX inhibition by compound 7 was also evaluated.

## Materials & methods

### Chemistry

#### General

Melting points (mps) were recorded uncorrected in open capillary tubes using Stuart melting point apparatus (Stuart Scientific, Redhill, UK). Infrared (IR) spectra of all newly synthesized compounds were reported using a Fourier transform IR spectrometer (Shimadzu, Tokyo, Japan). A Bruker 400 NMR spectrometer (Bruker Bioscience, MA, USA) was used at 400 and 100 MHz for recording  $^1\text{H}$  NMR and  $^{13}\text{C}$  NMR spectra, respectively. Tetramethylsilane (TMS) was used as an internal standard, while deuterated DMSO was used as a solvent. An HP Model EI-MS 5988 mass spectrometer (Hewlett Packard, CA, USA) was used to determine mass spectra. To obtain microanalytical values, a Carlo Erba 1108 Elemental Analyzer (Heraeus, Hanau, Germany) was used. For checking of reactions completion, precoated  $\text{SiO}_2$  gel (200 mesh, HF254) aluminum plates (Merck, Darmstadt, Germany) were used for thin layer chromatography (TLC), where a developing solvent system of chloroform/methanol (6.5:3.5) was used. Spots were visualized under UV light. Spectral and elemental analysis were consistent with the postulated structures. For purity inspection, high-performance liquid chromatography (HPLC) was used (Agilent 1260 Infinity apparatus, Agilent Technologies, Hewlett-Packard-Strasse 8 76337 Waldbronn, Germany) on ZORBAX Eclipse Plus C18 column (4.6  $\times$  100 mm, 3.5  $\mu\text{m}$ ) with a mobile phase acetonitrile:water mixture (60:40) at a flow rate of 1.0 ml/min; the detection wavelength was set at 250 nm.

#### 2-Cyano-N-(4-(N-(pyridin-2-yl)sulfamoyl)phenyl)acetamide (1)

Compound **1** was synthesized according to the reported procedure [61,62].

The general procedure for the preparation of 4-(6-amino-3,5-dicyano-2-oxo-4-substituted-pyridin-1(2H)-yl)-N-(pyridin-2-yl)benzenesulfonamides (**2–12**) was as follows.

A mixture of 2-cyano-N-(4-(N-(pyridin-2-yl)sulfamoyl)phenyl)acetamide **1** [59] (1.26 g, 0.004 mol) and the appropriate benzylidenemalononitrile (0.004 mol) was prepared in absolute ethanol (30 ml) with sodium ethoxide (prepared by dissolving 0.09 g of sodium metal in 5 ml absolute ethanol). The reaction mixture was refluxed for 8–10 h, then cooled and poured onto ice water and the medium was neutralized by dilute HCl. The precipitated solid was filtered off, washed with water and recrystallized from dioxane to give compounds **2–12**.

#### 4-(6-Amino-3,5-dicyano-2-oxo-4-phenylpyridin-1(2H)-yl)-N-(pyridin-2-yl)benzenesulfonamide (2)

Yield 78%; mp 250–252°C. IR ( $\text{cm}^{-1}$ ): 3320, 3230, 3200 (NH,  $\text{NH}_2$ ), 3046 (CH arom.), 2200 ( $\text{C}\equiv\text{N}$ ), 1680 ( $\text{C}=\text{O}$ ), 1285, 1110 ( $\text{SO}_2$ ).  $^1\text{H}$  NMR (DMSO- $d_6$ , ppm): 5.36 (s, 2H,  $\text{NH}_2$ , exchangeable with  $\text{D}_2\text{O}$ ), 6.35 (t, 1H,  $J = 8$  Hz, CH-pyridine), 6.45 (d, 2H,  $J = 8$  Hz, Ar-H), 6.61 (d, 1H,  $J = 8$  Hz, CH-pyridine), 7.17 (t, 1H,  $J = 8$  Hz, CH-pyridine), 7.28–7.32 (m, 3H, Ar-H), 7.43 (d, 4H,  $J = 8$  Hz, Ar-H), 7.87 (d, 1H,  $J = 8$  Hz, CH-pyridine), 10.93 (s, 1H, NH, exchangeable with  $\text{D}_2\text{O}$ ).  $^{13}\text{C}$  NMR (DMSO- $d_6$ , ppm): 77.11 (C-CN), 79.32 (C-CN), 112.53 (CN), 113.34 (CN), 115.06, 122.11, 127.34 (2), 129.06 (2), 130.29, 130.51, 130.59, 132.29, 134.59, 136.51, 137.67, 138.84, 152.86, 156.21, 157.36, 157.49, 161.41 (C- $\text{NH}_2$ ), 164.49 (C=O). EI-MS  $m/z$ : 468 ( $\text{M}^+$ ). Analysis calculated for  $\text{C}_{24}\text{H}_{16}\text{N}_6\text{O}_3\text{S}$ : C 61.53, H 3.44, N 17.94; found: C 61.67, H 3.74, N 17.86.

#### 4-(6-Amino-3,5-dicyano-2-oxo-4-(thiophen-2-yl)pyridin-1(2H)-yl)-N-(pyridin-2-yl)benzenesulfonamide (3)

Yield 75%; mp 271–273°C. IR ( $\text{cm}^{-1}$ ): 3322, 3231, 3202 (NH,  $\text{NH}_2$ ), 3048 (CH arom.), 2190 ( $\text{C}\equiv\text{N}$ ), 1690 ( $\text{C}=\text{O}$ ), 1315, 1105 ( $\text{SO}_2$ ).  $^1\text{H}$  NMR (DMSO- $d_6$ , ppm): 5.98 (s, 2H,  $\text{NH}_2$ , exchangeable with  $\text{D}_2\text{O}$ ), 6.56 (d, 1H,  $J = 8$  Hz, CH-pyridine), 6.83 (t, 1H,  $J = 8$  Hz, CH-pyridine), 7.18 (t, 1H,  $J = 8$  Hz, CH-pyridine), 7.53, 7.57 (2d, 4H,  $J = 8$  Hz, Ar-H), 7.64 (t, 1H,  $J = 8$  Hz, CH-thiophene), 8.09 (d, 1H,  $J = 8$  Hz, CH-pyridine), 8.54 (s, 1H, NH, exchangeable with  $\text{D}_2\text{O}$ ), 9.12, 9.32 (2d, 2H,  $J = 8$  Hz, 2CH-thiophene).  $^{13}\text{C}$  NMR (DMSO- $d_6$ , ppm): 73.88 (C-CN), 88.11 (C-CN), 112.66 (CN), 112.89 (CN), 119.42, 120.17, 125.44, 125.53, 126.72, 126.96, 127.67, 127.86 (CH-thiophene), 128.30 (C-thiophene), 128.52, 129.22 (CH-thiophene), 129.33, 139.17, 139.46 (CH-thiophene), 141.85, 151.25, 161.66 (C- $\text{NH}_2$ ), 162.66 (C=O). EI-MS  $m/z$ : 474 ( $\text{M}^+$ ). Analysis calculated for  $\text{C}_{22}\text{H}_{14}\text{N}_6\text{O}_3\text{S}_2$ : C 55.69, H 2.97, N 17.71; found: C 55.76, H 2.78, N 17.91.

#### 4-(6-Amino-3,5-dicyano-2-oxo-4-(p-tolyl)pyridin-1(2H)-yl)-N-(pyridin-2-yl)benzenesulfonamide (4)

Yield 69%; mp 262–264°C. IR ( $\text{cm}^{-1}$ ): 3319, 3232, 3202 (NH,  $\text{NH}_2$ ), 3047 (CH arom.), 2949, 2870 (CH aliph.), 2210 ( $\text{C}\equiv\text{N}$ ), 1720 ( $\text{C}=\text{O}$ ), 1259, 1125 ( $\text{SO}_2$ ).  $^1\text{H}$  NMR (DMSO- $d_6$ , ppm): 2.41 (s, 3H,  $\text{CH}_3$ ), 5.99 (s, 2H,  $\text{NH}_2$ , exchangeable with  $\text{D}_2\text{O}$ ), 6.56 (d, 1H,  $J = 8$  Hz, CH-pyridine), 6.90 (t, 1H,  $J = 8$  Hz, CH-pyridine), 7.08 (d, 2H,  $J = 8$  Hz, Ar-H), 7.32 (d, 2H,  $J = 8$  Hz, Ar-H), 7.53, 7.58 (2d, 4H,  $J = 8$  Hz, Ar-H), 7.67 (t,

1H,  $J = 8$  Hz, CH-pyridine), 8.08 (d, 1H,  $J = 8$  Hz, CH-pyridine), 9.32 (s, 1H, NH, exchangeable with D<sub>2</sub>O). <sup>13</sup>C NMR (DMSO-d<sub>6</sub>, ppm): 21.36 (CH<sub>3</sub>), 75.20 (C-CN), 76.23 (C-CN), 112.60 (CN), 112.88 (CN), 128.42, 128.64, 128.90, 129.09, 129.29, 129.36, 129.53, 129.69, 129.96, 130.73 (2), 132.18, 132.57, 133.48, 139.15, 139.23, 140.25, 140.73, 162.40, 166.50 (C=O). EI-MS  $m/z$ : 482 (M<sup>+</sup>). Analysis calculated for C<sub>25</sub>H<sub>18</sub>N<sub>6</sub>O<sub>3</sub>S: C 62.23, H 3.76, N 17.42; found: C 62.34, H 3.98, N 17.65.

#### 4-(6-Amino-3,5-dicyano-4-(4-fluorophenyl)-2-oxopyridin-1(2H)-yl)-N-(pyridin-2-yl)benzenesulfonamide (5)

Yield 82%; mp 258–260°C. IR (cm<sup>-1</sup>): 3327, 3235, 3250 (NH, NH<sub>2</sub>), 3045 (CH arom.), 2250 (C≡N), 1680 (C=O), 1262, 1130 (SO<sub>2</sub>). <sup>1</sup>H NMR (DMSO-d<sub>6</sub>, ppm): 6.78 (s, 2H, NH<sub>2</sub>, exchangeable with D<sub>2</sub>O), 7.26 (d, 1H,  $J = 8$  Hz, CH-pyridine), 7.32 (t, 1H,  $J = 8$  Hz, CH-pyridine), 7.39–7.50 (m, 4H, 4-F-phenyl), 7.57–7.59 (2d, 4H,  $J = 8$  Hz, Ar-H), 7.74 (t, 1H,  $J = 8$  Hz, CH-pyridine), 8.17 (d, 1H,  $J = 8$  Hz, CH-pyridine), 11.90 (s, 1H, NH, exchangeable with D<sub>2</sub>O). <sup>13</sup>C NMR (DMSO-d<sub>6</sub>, ppm): 72.89 (C-CN), 74.46 (C-CN), 102.69 (CN), 115.76 (CN), 116.09, 116.31, 116.57, 117.03, 117.25, 128.60 (2), 130.98 (2), 131.07 (2), 131.49, 134.15, 134.25, 154.32, 157.05, 160.16 (C-NH<sub>2</sub>), 162.06, 162.29 (C-F), 164.75 (C=O). EI-MS  $m/z$ : 486 (M<sup>+</sup>). Analysis calculated for C<sub>24</sub>H<sub>15</sub>FN<sub>6</sub>O<sub>3</sub>S: C 59.25, H 3.11, N 17.28; found: C 60.15, H 3.23, N 17.34.

#### 4-(6-Amino-3,5-dicyano-4-(4-methoxyphenyl)-2-oxopyridin-1(2H)-yl)-N-(pyridin-2-yl)benzenesulfonamide (6)

Yield 74%; mp 276–278°C. IR (cm<sup>-1</sup>): 3324, 3232, 3202 (NH, NH<sub>2</sub>), 3046 (CH arom.), 2949, 2870 (CH aliph.), 2200 (C≡N), 1690 (C=O), 1255, 1115 (SO<sub>2</sub>). <sup>1</sup>H NMR (DMSO-d<sub>6</sub>, ppm): 3.84 (s, 3H, OCH<sub>3</sub>), 5.88 (s, 2H, NH<sub>2</sub>, exchangeable with D<sub>2</sub>O), 6.56 (d, 1H,  $J = 8$  Hz, CH-pyridine), 6.68 (t, 1H,  $J = 8$  Hz, CH-pyridine), 6.86 (d, 2H,  $J = 8$  Hz, Ar-H), 7.31 (d, 2H,  $J = 8$  Hz, Ar-H), 7.52–7.68 (m, 3H, Ar-H, CH-pyridine), 7.87 (d, 2H,  $J = 8$  Hz, Ar-H), 8.02 (d, 1H,  $J = 8$  Hz, CH-pyridine), 9.20 (s, 1H, NH, exchangeable with D<sub>2</sub>O). <sup>13</sup>C NMR (DMSO-d<sub>6</sub>, ppm): 57.95 (OCH<sub>3</sub>), 74.64 (C-CN), 74.92 (C-CN), 111.95 (CN), 112.45 (CN), 112.76, 112.86, 115.37, 127.51, 127.80, 128.10, 128.20, 129.24, 129.26, 130.11, 137.67, 138.84, 152.86, 156.21, 157.36, 157.49, 158.48, 159.16 (C-OCH<sub>3</sub>), 161.41 (C-NH<sub>2</sub>), 165.59 (C=O). EI-MS  $m/z$ : 498 (M<sup>+</sup>). Analysis calculated for C<sub>25</sub>H<sub>18</sub>N<sub>6</sub>O<sub>4</sub>S: C 60.23, H 3.64, N 16.86; found: C 59.23, H 3.81, N 17.16.

#### 4-(6-Amino-4-(4-chlorophenyl)-3,5-dicyano-2-oxopyridin-1(2H)-yl)-N-(pyridin-2-yl)benzenesulfonamide (7)

Yield 89%; mp >280°C. IR (cm<sup>-1</sup>): 3330, 3230, 3201 (NH, NH<sub>2</sub>), 3048 (CH arom.), 2200 (C≡N), 1720 (C=O), 1228, 1108 (SO<sub>2</sub>), 825 (C-Cl). <sup>1</sup>H NMR (DMSO-d<sub>6</sub>, ppm): 5.85 (s, 2H, NH<sub>2</sub>, exchangeable with D<sub>2</sub>O), 6.49 (d, 1H,  $J = 8$  Hz, CH-pyridine), 6.65 (t, 1H,  $J = 8$  Hz, CH-pyridine), 7.34, 7.38, 7.42, 7.45 (4d, 8H,  $J = 8$  Hz, Ar-H), 7.55 (t, 1H,  $J = 8$  Hz, CH-pyridine), 8.01 (d, 1H,  $J = 8$  Hz, CH-pyridine), 9.24 (s, 1H, NH, exchangeable with D<sub>2</sub>O). <sup>13</sup>C NMR (DMSO-d<sub>6</sub>, ppm): 73.57 (C-CN), 73.94 (C-CN), 112.87 (CN), 117.65 (CN), 121.59, 127.48, 128.33, 128.65, 128.78, 128.94, 129.25, 129.31, 129.48, 130.36, 130.62, 130.83, 131.20, 132.47, 132.84, 133.22, 133.44, 133.49 (C-Cl), 161.30 (C-NH<sub>2</sub>), 166.14 (C=O). EI-MS  $m/z$ : 506 (M<sup>+</sup>), 508 (M<sup>+2</sup>). Analysis calculated for C<sub>24</sub>H<sub>15</sub>ClN<sub>6</sub>O<sub>3</sub>S: C 57.32, H 3.01, N 16.71; found: C 57.51, H 2.09, N 16.68.

#### 4-(6-Amino-3,5-dicyano-4-(4-(dimethylamino)phenyl)-2-oxopyridin-1(2H)-yl)-N-(pyridin-2-yl)benzenesulfonamide (8)

Yield 71%; mp 265–267°C. IR (cm<sup>-1</sup>): 3322, 3233, 3205 (NH, NH<sub>2</sub>), 3045 (CH arom.), 2949, 2870 (CH aliph.), 2210 (C≡N), 1626 (C=N), 1220, 1111 (SO<sub>2</sub>). <sup>1</sup>H NMR (DMSO-d<sub>6</sub>, ppm): 3.08 (s, 6H, 2CH<sub>3</sub>), 5.99 (s, 2H, NH<sub>2</sub>, exchangeable with D<sub>2</sub>O), 6.57 (d, 1H,  $J = 8$  Hz, CH-pyridine), 6.83 (d, 2H,  $J = 8$  Hz, Ar-H), 6.90 (t, 1H,  $J = 8$  Hz, CH-pyridine), 7.08 (d, 2H,  $J = 8$  Hz, Ar-H), 7.53 (d, 2H,  $J = 8$  Hz, Ar-H), 7.66 (t, 1H,  $J = 8$  Hz, CH-pyridine), 7.93 (d, 2H,  $J = 8$  Hz, Ar-H), 8.11 (d, 1H,  $J = 8$  Hz, CH-pyridine), 11.08 (s, 1H, NH, exchangeable with D<sub>2</sub>O). <sup>13</sup>C NMR (DMSO-d<sub>6</sub>, ppm): 41.40 (2CH<sub>3</sub>), 73.84 (C-CN), 74.88 (C-CN), 112.66 (CN), 112.87 (CN), 125.44, 125.53, 126.10, 126.17, 126.72, 126.96, 127.22, 127.46, 128.80, 128.95, 129.22, 129.33, 131.00, 135.06, 136.40, 139.17, 139.46, 141.85, 161.66, 162.66 (C=O). EI-MS  $m/z$ : 511 (M<sup>+</sup>). Analysis calculated for C<sub>26</sub>H<sub>21</sub>N<sub>7</sub>O<sub>3</sub>S: C 61.04, H 4.14, N 19.17; found: C 61.12, H 4.23, N 18.97.

#### 4-(6-Amino-4-(benzo[d][1,3]dioxol-5-yl)-3,5-dicyano-2-oxopyridin-1(2H)-yl)-N-(pyridin-2-yl)benzenesulfonamide (9)

Yield 80%; mp >280°C. IR (cm<sup>-1</sup>): 3321, 3236, 3203 (NH, NH<sub>2</sub>), 3048 (CH arom.), 2200 (C≡N), 1720 (C=O), 1232, 1105 (SO<sub>2</sub>). <sup>1</sup>H NMR (DMSO-d<sub>6</sub>, ppm): 6.16 (s, 2H, NH<sub>2</sub>, exchangeable with D<sub>2</sub>O), 6.21 (s, 2H, CH<sub>2</sub>-dioxole), 6.84–7.10 (m, 5H, Ar-H, 2CH-pyridine), 7.14 (t, 1H,  $J = 8$  Hz, CH-pyridine), 7.52 (d, 2H,  $J = 8$  Hz, Ar-H), 7.68 (d, 2H,  $J = 8$  Hz, Ar-H), 8.29 (d, 1H,  $J = 8$  Hz, CH-pyridine), 10.53 (s, 1H, NH, exchangeable with D<sub>2</sub>O). <sup>13</sup>C NMR (DMSO-d<sub>6</sub>, ppm): 72.73 (C-CN), 73.92 (C-CN), 102.87 (CH<sub>2</sub>-dioxol),

112.87 (CN), 117.65 (CN), 128.33, 128.65, 128.78, 128.94, 129.31, 129.48, 130.62, 130.83, 131.20, 132.47, 132.84, 133.22, 133.44, 133.49, 135.46, 135.66, 137.89, 139.14, 161.30 (C-NH<sub>2</sub>), 166.17 (C=O). EI-MS *m/z*: 512 (M<sup>+</sup>). Analysis calculated for C<sub>25</sub>H<sub>16</sub>N<sub>6</sub>O<sub>5</sub>S: C 58.59, H 3.15, N 16.40; found: C 58.49, H 3.35, N 16.56.

#### 4-(6-Amino-3,5-dicyano-4-(4-nitrophenyl)-2-oxopyridin-1(2H)-yl)-N-(pyridin-2-yl)benzenesulfonamide (10)

Yield 77%; mp 274–276°C. IR (cm<sup>-1</sup>): 3332, 3223, 3210 (NH, NH<sub>2</sub>), 3047 (CH arom.), 2190 (C≡N), 1690 (C=O), 1222, 1117 (SO<sub>2</sub>). <sup>1</sup>H NMR (DMSO-d<sub>6</sub>, ppm): 5.98 (s, 2H, NH<sub>2</sub>, exchangeable with D<sub>2</sub>O), 6.57 (d, 1H, *J* = 8 Hz, CH-pyridine), 6.90 (t, 1H, *J* = 8 Hz, CH-pyridine), 7.09 (d, 2H, *J* = 8 Hz, Ar-H), 7.54 (d, 2H, *J* = 8 Hz, Ar-H), 7.65 (t, 1H, *J* = 8 Hz, CH-pyridine), 7.70 (d, 2H, *J* = 8 Hz, Ar-H), 8.11 (d, 2H, *J* = 8 Hz, Ar-H), 8.41 (d, 1H, *J* = 8 Hz, CH-pyridine), 10.67 (s, 1H, NH, exchangeable with D<sub>2</sub>O). <sup>13</sup>C NMR (DMSO-d<sub>6</sub>, ppm): 73.87 (C-CN), 77.11 (C-CN), 112.66 (CN), 112.87 (CN), 119.42, 120.17, 125.44, 125.53, 126.72, 126.96, 127.65, 127.86, 128.30, 128.52, 129.22, 129.33, 131.00, 135.06, 139.17, 139.46, 141.85, 151.25 (C-NO<sub>2</sub>), 161.66 (C-NH<sub>2</sub>), 162.66 (C=O). EI-MS *m/z*: 513 (M<sup>+</sup>). Analysis calculated for C<sub>24</sub>H<sub>15</sub>N<sub>7</sub>O<sub>5</sub>S: C 56.14, H 2.94, N 19.09; found: C 55.04, H 1.84, N 19.89.

#### 4-(6-Amino-3,5-dicyano-4-(4-hydroxy-3-methoxyphenyl)-2-oxopyridin-1(2H)-yl)-N-(pyridin-2-yl)benzenesulfonamide (11)

Yield 65%; mp 267–279°C. IR (cm<sup>-1</sup>): 3420 (OH), 3329, 3235, 3209 (NH, NH<sub>2</sub>), 3048 (CH arom.), 2939, 2880 (CH aliph.), 2200 (C≡N), 1720 (C=O), 1230, 1108 (SO<sub>2</sub>). <sup>1</sup>H NMR (DMSO-d<sub>6</sub>, ppm): 3.83 (s, 3H, OCH<sub>3</sub>), 3.92 (s, 2H, NH<sub>2</sub>, exchangeable with D<sub>2</sub>O), 6.84 (t, 1H, *J* = 8 Hz, CH-pyridine), 7.06 (d, 1H, *J* = 8 Hz, CH-pyridine), 7.30 (t, 1H, *J* = 8 Hz, CH-pyridine), 7.68 (d, 4H, *J* = 8 Hz, Ar-H), 7.76–7.96 (m, 3H, Ar-H), 8.20 (d, 1H, *J* = 8 Hz, CH-pyridine), 9.17 (s, 1H, NH, exchangeable with D<sub>2</sub>O), 10.41 (s, 1H, OH, exchangeable with D<sub>2</sub>O). <sup>13</sup>C NMR (DMSO-d<sub>6</sub>, ppm): 56.06 (OCH<sub>3</sub>), 77.95 (C-CN), 79.38 (C-CN), 112.53 (CN), 113.92 (CN), 115.87, 122.11, 127.34 (2), 129.06 (2), 130.11, 130.12, 130.34, 132.29, 134.59, 136.51, 137.67, 138.84, 152.86, 156.21 (C-OH), 157.36, 157.49, 161.41 (C-NH<sub>2</sub>), 165.59 (C=O). EI-MS *m/z*: 514 (M<sup>+</sup>). Analysis calculated for C<sub>25</sub>H<sub>18</sub>N<sub>6</sub>O<sub>5</sub>S: C 58.36, H 3.53, N 16.33; found: C 58.57, H 3.64, N 16.23.

#### 4-(6-Amino-3,5-dicyano-4-(2,4-dichlorophenyl)-2-oxopyridin-1(2H)-yl)-N-(pyridin-2-yl)benzenesulfonamide (12)

Yield 86%; mp >280°C. IR (cm<sup>-1</sup>): 3320, 3230, 3200 (NH, NH<sub>2</sub>), 3045 (CH arom.), 2190 (C≡N), 1680 (C=O), 1315, 1105 (SO<sub>2</sub>), 835 (C-Cl). <sup>1</sup>H NMR (DMSO-d<sub>6</sub>, ppm): 5.98 (s, 2H, NH<sub>2</sub>, exchangeable with D<sub>2</sub>O), 6.56 (d, 1H, *J* = 8 Hz, CH-pyridine), 6.90 (t, 1H, *J* = 8 Hz, CH-pyridine), 6.99 (t, 1H, *J* = 8 Hz, CH-pyridine), 7.07, 7.13 (2d, 2H, *J* = 8 Hz, Ar-H), 7.53, 7.57 (2d, 4H, *J* = 8 Hz, Ar-H), 7.81 (s, 1H, Ar-H), 8.10 (d, 1H, *J* = 8 Hz, CH-pyridine), 8.24 (s, 1H, NH, exchangeable with D<sub>2</sub>O). <sup>13</sup>C NMR (DMSO-d<sub>6</sub>, ppm): 75.59 (C-CN), 89.66 (C-CN), 112.63 (CN), 112.90 (CN), 114.98, 115.83, 129.62, 129.85, 129.92, 130.10, 131.53, 131.91, 132.26, 133.25, 134.59, 136.04 (C-Cl), 136.51, 137.68 (C-Cl), 139.27, 152.77, 153.19, 157.14, 159.70, 159.98 (C=O). EI-MS *m/z*: 537 (M<sup>+</sup>), 539 (M<sup>+2</sup>). Analysis calculated for C<sub>24</sub>H<sub>14</sub>Cl<sub>2</sub>N<sub>6</sub>O<sub>3</sub>S: C 53.64, H 2.63, N 15.64; found: C 53.54, H 2.45, N 15.56.

## Irradiation

Dry pure compound 7, in the solid state, was gathered in polyethylene vials covered with an aluminum sheath and exposed to γ-rays at an absorbed dose of 25 kGy. Irradiation was performed using a <sup>60</sup>Co source at a dose rate of 1.208 kGy/h using a 4000A gamma chamber (Sheridan science and technology park, ON, Canada).

## Molecular docking

The protein structure of CA IX was retrieved from PDB (PDB ID: 7POM) [63,64]. The protein structure was prepared by removing water molecules, deleting all chains except chain A and removing co-crystallized ligands and other small molecules through AutoDock Tools v. 1.5.6 [65]. Then the protein .pdb file was converted to pdbqt format by assigning charges through the prepare\_receptor4.py script from AutoDock Tools 1.5.7. The Zn-repulsive component is mediated by the zinc atom, while the attractive component is mediated by a TZ pseudoatom generated by zinc\_pseudo.py script [66]. The GetBox PyMOL plugin (Schrödinger, L., & DeLano, W. [2020]. PyMOL. Retrieved from <http://www.pymol.org/pymol>) was used to determine the search space by selecting the co-crystallized ligand for centering the box around, with the center at -27, 12.7, -27 and dimensions of 25 Å. The prepare\_gpf4zn.py script was used for generating a receptor grid file for generating the grid maps by autogrid4. Ligands were sketched by MarvinSketch, (Marvin version 21.17.0, ChemAxon [<https://www.chemaxon.com>]) then converted to 3D and energy minimized using OpenBabel 2.4.1 [67] via a steepest descent minimization algorithm

for 10,000 steps and a convergence criterion of  $10^{-6}$  kcal/mol/Å, implementing MMFF94s (Merck Molecular Force Field static variant) for stepwise energy calculations [68]. The `mk_prepare_ligand.py` script was then used to prepare the ligands. Finally, AutoDock Vina v. 1.2.3 [69] was used for docking calculations. All protein–ligand figure generation was done using UCSF Chimera visualization software [70].

## Biological evaluation

### *Cell culture*

All selected cell lines for breast cancer – MCF-7 (breast adenocarcinoma), T-47D (breast ductal carcinoma) and MDA-MB-231 (breast cancer) – were grown in Nawah Scientific Labs (Mokatam, Cairo, Egypt). All the cells were grown in Dulbecco's modified Eagle medium enriched with 10% fetal bovine serum, 100 U/ml penicillin and 100 mg/ml streptomycin. The cells were kept in a humidified atmosphere at 37°C with 5% CO<sub>2</sub>.

### *Cytotoxicity assay*

To evaluate the cytotoxicity of the synthesized compounds, a sulforhodamine B ([SRB], was purchased from Sigma Aldrich Company, MO, USA) cell viability assay was carried out. Five serial dilutions (0.01, 0.1, 1, 10 and 100 μM) of the tested compounds were tested against 3000–5000 cells, which were seeded in 96-well plates before treatment within 24 h. Each well in the 96-well plate was seeded with 100 μl containing 3000–5000 cells. Then after 24 h another 100 μl was added to each well containing five serial dilutions (0.01, 0.1, 1, 10, and 100 μM) of the tested compounds. After 72 h incubation, the medium was discarded and Trichloroacetic acid ([TCA], which was purchased from Sigma Aldrich Company, USA) (10% w/v) was added to for fixation, followed by washing, then staining with 70 μl of SRB solution (0.4% w/v) which was left on the cells for 10 min. Afterward, the wells were washed with acetic acid (1% v/v). The absorbance of the accrued color by the bound SRB was measured after adding 100 μl Tris buffer (10 mM) at 540 nm using a BMG LABTECH®-FLUOstar Omega microplate reader (Ortenberg, Germany). The generated viability for each concentration was fitted to nonlinear regression to generate the dose–response curve.

### *Analysis of cell cycle distribution*

All three cell lines were treated with the selected compound for 48 h. After treatment, cells were collected and washed twice with phosphate-buffered saline (PBS; pH 7.4). After washing, cells were incubated for 1 h at 4°C with 60% ice-cold ethanol for fixation. After fixation, the cells were washed with PBS and then resuspended in 1 ml of PBS containing 50 μg/ml RNase A and 10 μg/ml propidium iodide (PI) for staining. Cells were left for 20 min in the dark with the staining solution, then injected into a flow cytometer for DNA quantification using FL2 (λ<sub>ex</sub>/em 535/617 nm) signal detector (ACEA Novocyte™ flow cytometer, ACEA Biosciences Inc., CA, USA). For each sample, 12,000 events were measured and gated to analyze the cell cycle distribution using ACEA NovoExpress™ software (ACEA Biosciences Inc.).

### *Apoptosis assessment*

Cells from the selected cell lines were treated with compound 7 for 48 h. After treatment, cells were harvested using trypsin–EDTA, then washed twice with PBS. After washing, 10<sup>5</sup> cells were stained with annexin V–fluorescein isothiocyanate (FITC) apoptosis detection kit (Abcam, Inc., Cambridge, UK) and incubated in the dark for 30 min. For evaluation of apoptotic and necrotic populations, two fluorescent channels were assigned using flow cytometry. After the staining time, cells were analyzed using the ACEA Novocyte flow cytometer and evaluated for FITC and PI fluorescent signals (λ<sub>ex</sub>/em 488/530 nm for FITC and λ<sub>ex</sub>/em 535/617 nm for PI, respectively). Finally, the data were computed to quadrant analysis and calculated using ACEA NovoExpress software.

### *Autophagy assessment*

Autophagic cell death for the tested cell lines was measured using acridine orange lysosomal stain followed by quantification using flow cytometry. After 48 h of treatment, 10<sup>5</sup> cells were harvested and washed with PBS (pH 7.4). Cells were left for a 30-min incubation with the stain in a dark place at 37°C. After staining, autophagy for the selected cell lines was measured via ACEA Novocyte flow cytometer, and autophagic fluorescent signals were analyzed using signal detector (λ<sub>ex</sub>/em 488/530 nm) in triplicate; 12,000 events were acquired to produce net fluorescence intensities and quantified by ACEA NovoExpress software.

*Wound healing assay*

For the wound healing assay, cells were seeded at a density of  $2 \times 10^5$  cells per well onto a coated 12-well plate and cultured overnight in 5% fetal bovine serum-supplemented Dulbecco's modified Eagle medium at 37°C and 5% CO<sub>2</sub>. After 24 h of seeding, horizontal scratches were made into the fully confluent monolayer. The plate was then washed thoroughly with PBS to remove detached cells because of scratching, followed by replenishing all wells with fresh medium; wells that contained the drug were replenished with media containing the drug. Images of the wound were taken at 0, 24, 48, and 72 h. Then the plate was incubated at 37°C and 5% CO<sub>2</sub> for the full course of the experiment. The acquired images were analyzed by MII ImageView software v. 3.7 (Informer technologies Inc., CA, USA). The gap produced as result of the scratch was measured at the same time intervals and was compared with the initial gap at time  $t = 0$ . Wound closure percentage was calculated from the following equation:

$$\text{Wound closure\%} : \left( \frac{\text{wt} = 0\text{hr} - \text{wt} = \Delta\text{h}}{\text{wt} = 0\text{h}} \right) \times 100$$

wt = 0 hr is the average area of the wound measured immediately after scratching (time zero),  
wt = Δh is the average area of the wound measured h hours after the scratch is performed.

*CA IX inhibition assay*

The inhibitory effect of compound **7** against CA IX was assessed using the Carbonic Anhydrase Inhibitor Screening Kit (catalog # K473–100, BioVision™, CA, USA) with the use of purchased CA IX protein (AA 1–459, GST tag; catalog # ABIN1347791, Antibodies-Online GmbH, Aachen, Germany). The assay was done following the recommendation of the assay kit manufacturer. In brief, compound **7** as well as dorzolamide HCl (as positive control) were dissolved at 10× final concentration in DMSO and incubated with the enzyme and the assay buffer for 10 min at room temperature, then 5 μl of enzyme substrate were added and mixed well. Finally, absorbance was measured at 405 nm in a kinetic mode for 1 h at room temperature. Slopes were calculated from the linear range. All experiments were done as three independent replicates and results were reported as mean ± SD.

**Statistical analysis**

All conducted experiments were independently performed at least three times and the results reported as mean with SD. All compounds' IC<sub>50</sub> values were calculated using GraphPad Prism v. 8.0.1. (GraphPad, Inc., CA, USA).

**Results****Irradiation & purity**

Compound **7** was exposed to γ-radiation [71,72] in an attempt to study its chemical stability. It was irradiated at 25 kGy as a single dose [73] in its solid state [74,75]. The physicochemical properties of compound **7** were compared within days after irradiation, and it was observed that there was no difference in the physicochemical properties of compound **7** before and after irradiation. There was no change in solubility, odor, color or form.

TLC and HPLC were used to evaluate the purity of the irradiated compound **7** [75]. No change in R<sub>f</sub> values and no additional spots were observed with TLC. Close purity percentages of compound **7** were perceived with HPLC before and after the irradiation process (Supplementary Figure 1A & B).

**Molecular docking**

Molecular docking studies were carried out to investigate the potential binding pose of tested compounds with CA IX. The crystal structure of CA IX with PDB ID 7POM was chosen for the docking study as it shows the human variant for CA IX, which conforms with our *in vitro* studies on human CA IX. Also, it is of good resolution (1.98 Å) co-crystallized with a ligand, hence facilitating the identification of the binding site, and is the most recent CA IX PDB crystal structure. Because CA is a zinc metalloprotein, AutoDock Vina was used for docking [69], implementing the AutoDock4Zn force field [66] and AutoDock 4 scoring function [76]. First, the docking protocol was validated by redocking the co-crystallized ligand and measuring the root mean square deviation (RMSD) between the docked and co-crystallized poses. The root mean square deviation was found to be 1.4 Å, as calculated by DockRMSD server [77], which reflects the accepted docking power of the used software (Figure 1A). The co-crystallized ligand had a docking score of -32.034 kcal/mol. The docked pose reproduced the main binding interactions formed by

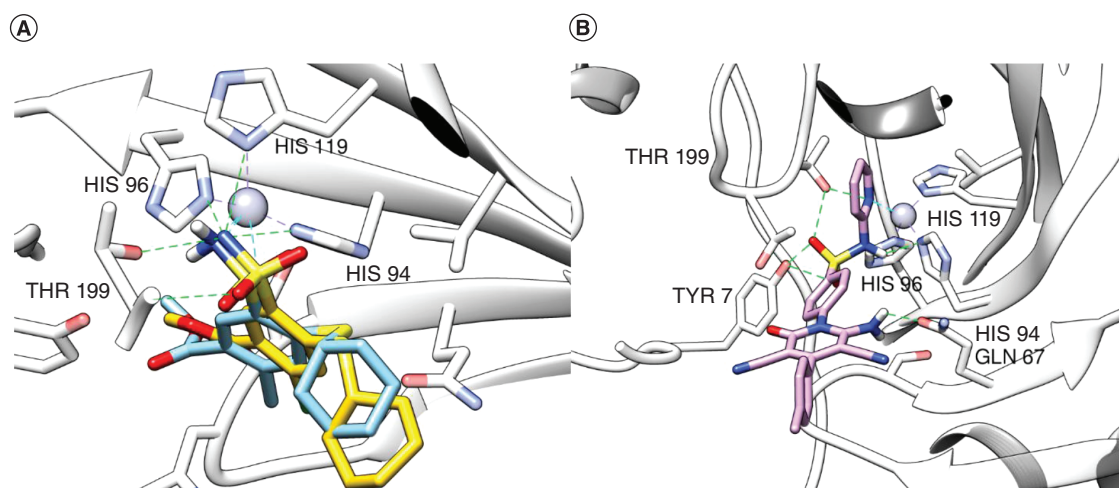


**Figure 3.** 3D interaction diagram. (A) 3D interaction diagram for CA IX (Protein Data Bank ID: 7POM) (gray) with sulfonamide cocrystallized ligand (yellow) and its docked pose (cyan). (B) 3D interaction diagram for CA IX (gray) with compound 7 (violet). Coordination of histidine triad with zinc in gray dashed lines, coordination of compounds with zinc in cyan dashed lines and conventional hydrogen bonds in green dashed lines.

**Table 1.** IC<sub>50</sub> values for the tested compounds against three cell lines (MCF-7, T47D and MDA-MB231).

Compound	IC <sub>50</sub> (μM)		
	MCF-7	T47D	MDA-MB231
1	>100	>100	>100
2	>100	>100	>100
3	40.52	34.18	58.36
4	>100	>100	>100
5	77.25	73.95	99.89
6	>100	>100	>100
7	12.15	14.43	23.82
8	>100	>100	>100
9	>100	>100	>100
10	>100	>100	>100
11	61.05	95.95	99.76
12	>100	>100	>100
Doxorubicin	0.6181	0.52	0.566

the co-crystallized ligand, including three hydrogen bonds with the histidine triad of His94, His96 and His119, and two hydrogen bonds with Thr199 backbone NH and side chain OH groups. The metal interaction with Zn<sup>2+</sup>, coordinated with the histidine triad, was also retained by the docked pose (Figure 3A).

## Biological evaluation

### Cytotoxicity effects

The SRB assay was selected to evaluate the cytotoxicity of 11 novel synthesized compounds (2–12) and the starting compound 1 on three different breast tumor cell lines (MCF-7, T47D and MDA-MB231). Five concentrations (0.01, 0.1, 1.0, 10.0 and 100 μM) were used to draw the dose–response curve for the 11 compounds on different cell lines, using doxorubicin as the reference drug.

Four compounds (3, 5, 7 and 11) out of the 12 tested showed cytotoxicity against the three cell lines, with IC<sub>50</sub> values ranging from 12.15 to 99.95 μM. Compound 7 showed the most cytotoxic activity, with IC<sub>50</sub> values of 12.15, 14.43 and 23.82 μM against MCF-7, T47D and MDA-MB231, respectively. Other compounds exhibited IC<sub>50</sub> values of >100 μM (Figure 4 & Table 1). Accordingly, compound 7 was selected for additional investigations [78].

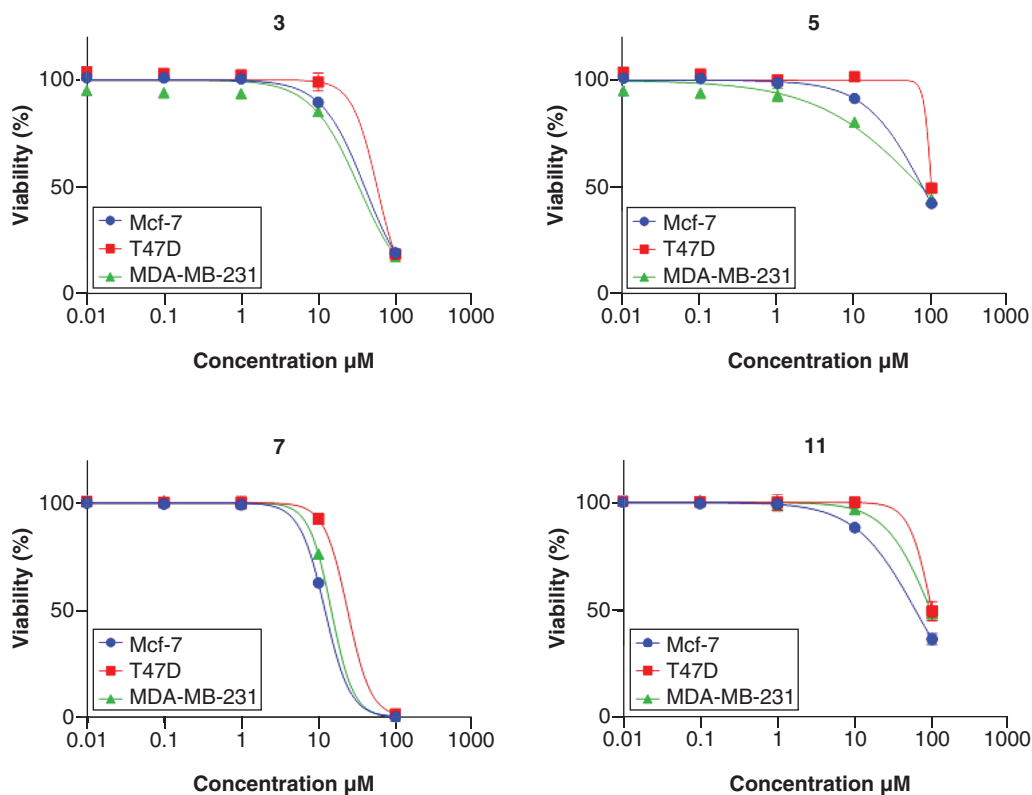


**Figure 4.** The dose–response curve for the four active compounds (3, 5, 7 and 11). 12 compounds were tested in total. The three cell lines (MCF-7, T47D and MDA-MB23) were exposed to serial dilutions of the tested compounds for 72 h, then cell viability was evaluated by a sulforhodamine-B assay. Data are shown as mean  $\pm$  SD ( $n = 3$ ).

#### Assessment of cell cycle distribution

Using flow cytometry, the effect of compound 7 on cell cycle progression was studied [79,80] in the three cell lines (MCF-7, T47D and MDA-MB23). In MCF-7 cells, compound 7 was found to increase the G1 population from 54.30% (untreated cells) to 60.19%, indicating that it arrested the cell cycle at the G1 phase. Similarly, in the T47D cell line, compound 7 significantly accumulated cells in the G1 phase from 55.32 to 72.69%; and in MDA-MB231 the percentage of cells in the G1 phase increased from 43.27 to 55.12% (Figure 5).

#### Apoptosis evaluation

In order to study apoptotic and necrotic populations, the three cell lines were treated with  $IC_{50}$  values of compound 7 for 48 h using annexin-v/FITC–PI [81] and flow cytometry (Figure 6). Compound 7 treatment led to a significant change in the percentage of apoptosis and total cell death (i.e., apoptosis and necrosis) compared with untreated control cells. In the MCF-7 cell line, these percentages were  $5.06 \pm 0.37\%$  and  $7.50 \pm 0.38\%$ , respectively; in the T47D cell line they were  $4.45 \pm 0.08\%$  and  $7.29 \pm 0.39\%$ , respectively; and in the MDA-MB231 cell line they were  $6.48 \pm 1.07\%$  and  $8.00 \pm 1.27\%$ , respectively. Consequently, compound 7 was further tested for its effects on autophagic cell death.

#### Autophagic assessment

Apart from apoptosis, programmed cell death via autophagy was evaluated using acridine orange stain and flow cytometry [82]. We further investigated the effect of compound 7  $IC_{50}$  on the autophagy process on the three cell lines MCF-7, T47D and MDA-MB231 (Figures 7). In the MCF-7 cell line, compound 7 increased autophagic cell death by 6.57%, while in T47D and MDA-MB231 compound 7 had a more potent effect, increasing autophagic cell death by 66.82 and 62.00%, respectively, compared with the control untreated cell line.

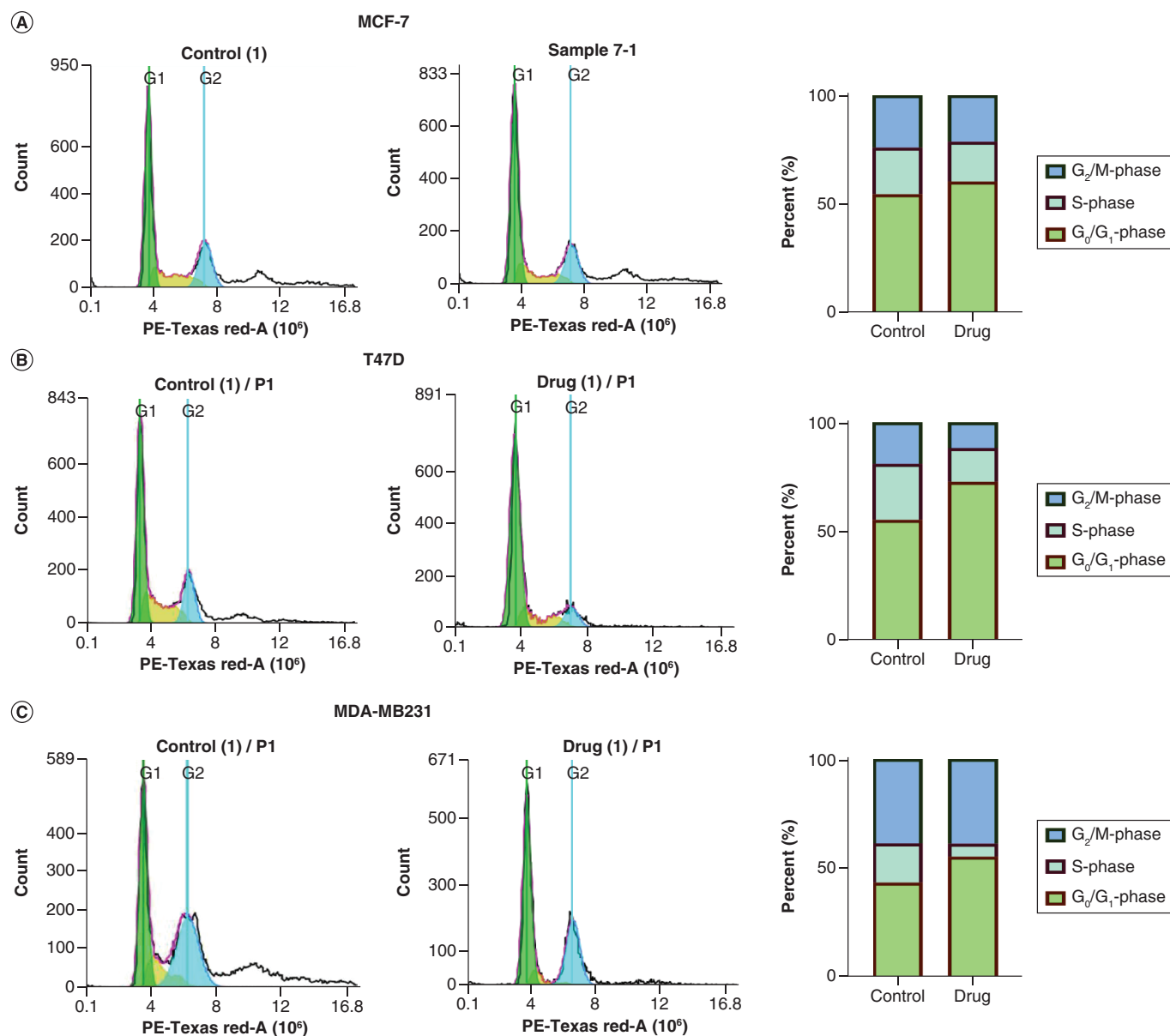


**Figure 5.** Effect of predetermined  $IC_{50}$  values of compound 7 on the cell cycle distribution of MCF-7, T47D and MDA-MB231 cell lines. Cells were incubated with the compound for 48 h, and cells' distribution over the three phases was evaluated via DNA quantification by flow cytometry. The percentage of cells in each phase was plotted as a percentage of total events, as shown in the bar chart. (A) MCF-7. (B) T47d. (C) MDA-MB231.

#### Wound healing assessment

The cytotoxic effect of compound 7 on the three tested cell lines led to the evaluation of its antimigratory effect [83]. Compound 7 delayed the migration of MCF-7, T47D and MDA-MB231 cells, as shown in Table 2 & Figure 8. The results showed that the antimigratory effect of compound 7 was more potent on MCF-7 and T47d cell lines compared with the MDA-MB231 cell line. T47D was the most sensitive cell line to the antimigratory effect of compound 7.

#### CA IX inhibition assay

Compound 7 showed good results against cancer cell lines. In addition, docking results supported its role as a CA IX inhibitor, so we were interested to confirm its inhibitory effect using an enzyme assay. Compound 7 showed

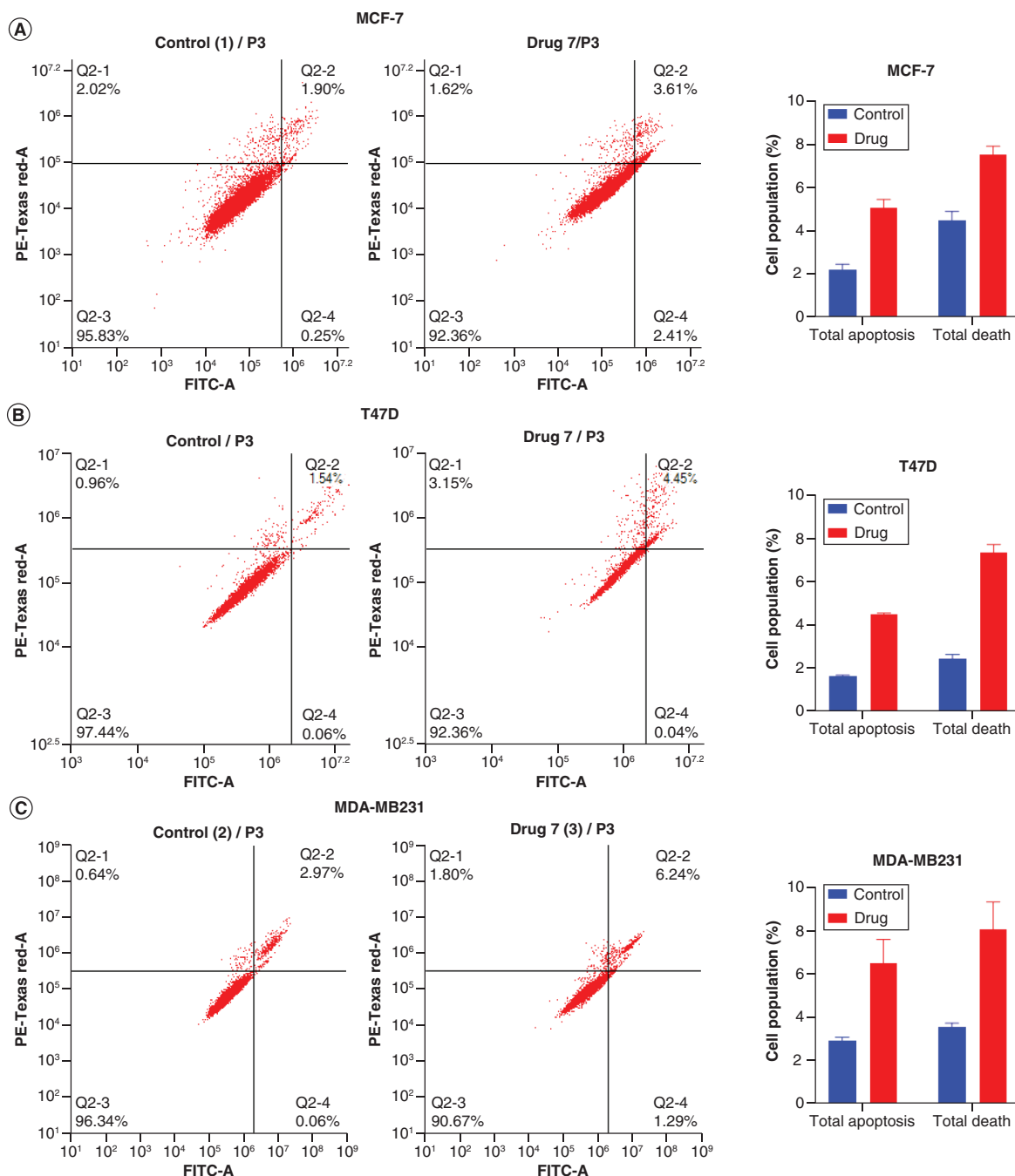


**Figure 6.** Effect of compound 7 on apoptosis in MCF-7, T47D and MDA-MB231 cell lines. Cells were incubated with the compound for 48 h, and all three cell lines were stained with annexin V/fluorescein isothiocyanate/propidium iodide. The four quadrants represent cells in normal, early, late and necrosis stages. Data represent a comparison of apoptosis and total cell death in both control and drug-treated groups. (A) MCF-7. (B) T47d. (C) MDA-MB231.

moderate inhibition of CA IX ( $253 \pm 12$  nM) compared with dorzolamide ( $122 \pm 6$  nM) which is a known CA inhibitor.

## Discussion Chemistry

In an attempt to explore new compounds for treating challenging breast cancer, a new series of 4-(6-amino-3,5-dicyano-2-oxo-4-substituted-pyridin-1(2H)-yl)-N-(pyridin-2-yl)-benzenesulfonamides was synthesized in this

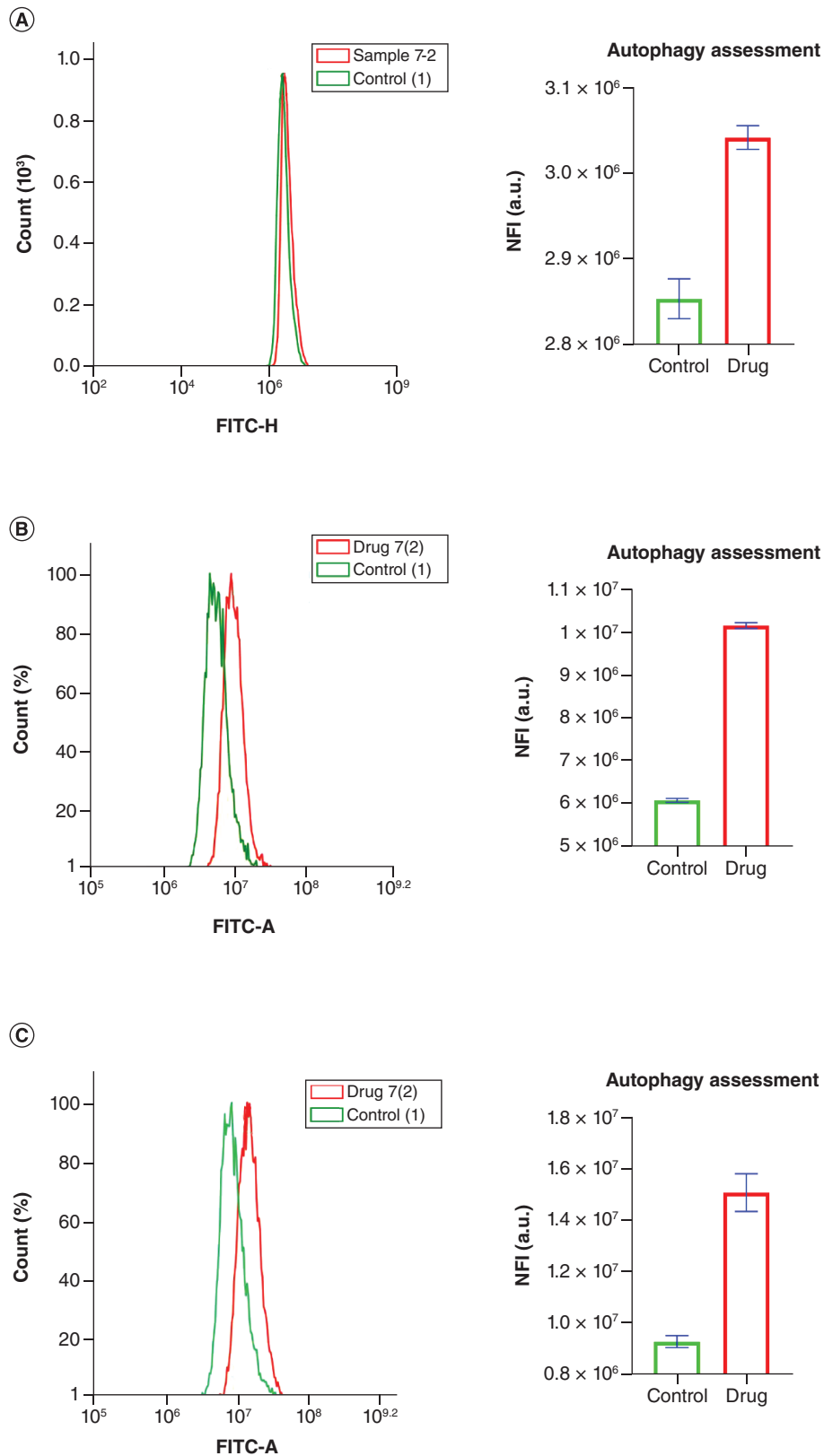


**Figure 7.** Effect of compound 7 on autophagic cell death in MCF-7, T47D and MDA-MB231 cell lines. Cells were incubated with the compound for 48 h, and net fluorescence intensity of treated cells was compared with the fluorescence of the control group. **(A)** MCF-7. **(B)** T47d. **(C)** MDA-MB231. NFI: Net fluorescence intensity.

Table 2. Wound closure percentage for MCF-7, T47D and MDA-MB231 cell lines after exposure to compound 7 at different time points.

Duration	Wound closure %					
	MCF-7		T47d		MDA-MB-231	
	Control %	Drug %	Control %	Drug %	Control %	Drug %
0 h	0	0	0	0	0	0
24 h	53.57 ± 4.09	30.35 ± 6.03	39.37 ± 4.33	20.88 ± 1.11	72.92 ± 11.98	49.68 ± 18.9
48 h	91.87 ± 2.7	46.25 ± 11.98	65.68 ± 5.57	29.8 ± 6.01	100 ± 0	69.53 ± 18.13
72 h	100 ± 0	76.69 ± 14.38	100 ± 0	46.64 ± 5.1	100 ± 0	100 ± 0

work, as shown in Figure 9. 2-Cyano-N-(4-(N-(pyridin-2-yl)sulfamoyl)phenyl)acetamide (**1**) was used as starting material and was synthesized according to the reported method [59,60]. This compound was then reacted with appropriate benzylidenemalononitrile in refluxing sodium ethoxide to give compounds **2–12** in yields that were good or very good. The structures of all newly synthesized compounds were verified via spectral and elemental analysis. All spectral data confirmed the disappearance of the aliphatic CH<sub>2</sub> signal of the starting compound **1**. Furthermore, the introduction of an NH<sub>2</sub> group in compounds **2–12** was confirmed through the appearance of new bands in IR spectra, as well as the exhibition of a singlet signal in <sup>1</sup>H NMR spectra, exchangeable with D<sub>2</sub>O at 3.98–6.78 ppm. Additionally, <sup>13</sup>C NMR spectra of compounds **2–12** displayed downfield signal at 159.70–162.40 ppm, ascribed to the introduced NH<sub>2</sub>. All the above mentioned signals confirmed cyclization with the postulated benzylidenes. <sup>1</sup>H NMR spectra of compounds **4**, **6**, **8** and **11** showed extra singlet signals at 2.41, 3.84, 3.08 and 3.83 ppm, respectively, assigned to the introduced methyl and methoxy groups and confirming reaction with the corresponding benzylidene. In addition, the <sup>1</sup>H NMR spectrum of compound **11** revealed an extra downfield signal exchangeable with D<sub>2</sub>O, corresponding to the introduced OH group. <sup>13</sup>C NMR spectra displayed extra signals for all aromatic carbons introduced at the identified positions. In addition, <sup>13</sup>C NMR spectra of compounds **4**, **6**, **8** and **11** revealed the most upfield signals at 21.36, 57.95, 41.40 and 56.06 ppm respectively, assigned to the introduced methyl and methoxy groups and confirming the specified reactions. Additionally, all mass spectra and elemental analysis results were in accordance with the postulated structures.

### Irradiation & purity

Gamma irradiation can be used as a means of sterilization in the pharmaceutical industry, so irradiation of newly synthesized compounds as potential future drugs is performed to evaluate their chemical stability. According to the results shown in Supplementary Figure 1A & B, the p-chloro derivative **7** could be considered radiostable, as it experienced no critical changes in its physicochemical properties upon irradiation.

### Molecular docking

According to the docking scores of the tested compounds (shown in Supplementary Table 1), compound **7** showed the best docking energy of -30.143 kcal/mol, comparable to that of the co-crystallized ligand and reflecting its strong interactions with the protein. These results support the superiority of compound **7** in the cytotoxicity assays. Compound **7** retained the coordination to the Zn<sup>2+</sup> metal through the nitrogen atom of the pyridine group, which also formed a hydrogen bond with Thr199 (Figure 3B).

Although the co-crystallized ligand interacts with the Zn ion through the sulfonamide terminal group, the docking predicted our designed compound to coordinate with the Zn ion through the nitrogen atom of the terminal pyridine ring. This can be attributed to the fact that the sulfonamide group in our compound is not terminal and the binding site at the histidine triad cannot accommodate the bulky pyridine group in order to enable the sulfonamide to bind with the Zn atom as noticed in the co-crystallized ligand. Four hydrogen bonds were formed with the sulfonamide group: one via a sulfonamide NH group with His94, and three by SO<sub>2</sub> groups with Tyr7 and Thr199. It also formed π-sulfur interactions with Tyr7 and His96 residues (Supplementary Figure 1). The compound's amino group formed an additional hydrogen bonding interaction with Gln67. These interactions account for the stability of the compound **7** docked pose and its good docking score.

### Biological evaluation

Compound **7** arrested the cell cycle progression of T47D, MCF-7 and MDA-MB231 cells at the G1 phase, indicating its antiproliferative effect on the three cell lines. Our results also correlated with previous findings [84,85] that

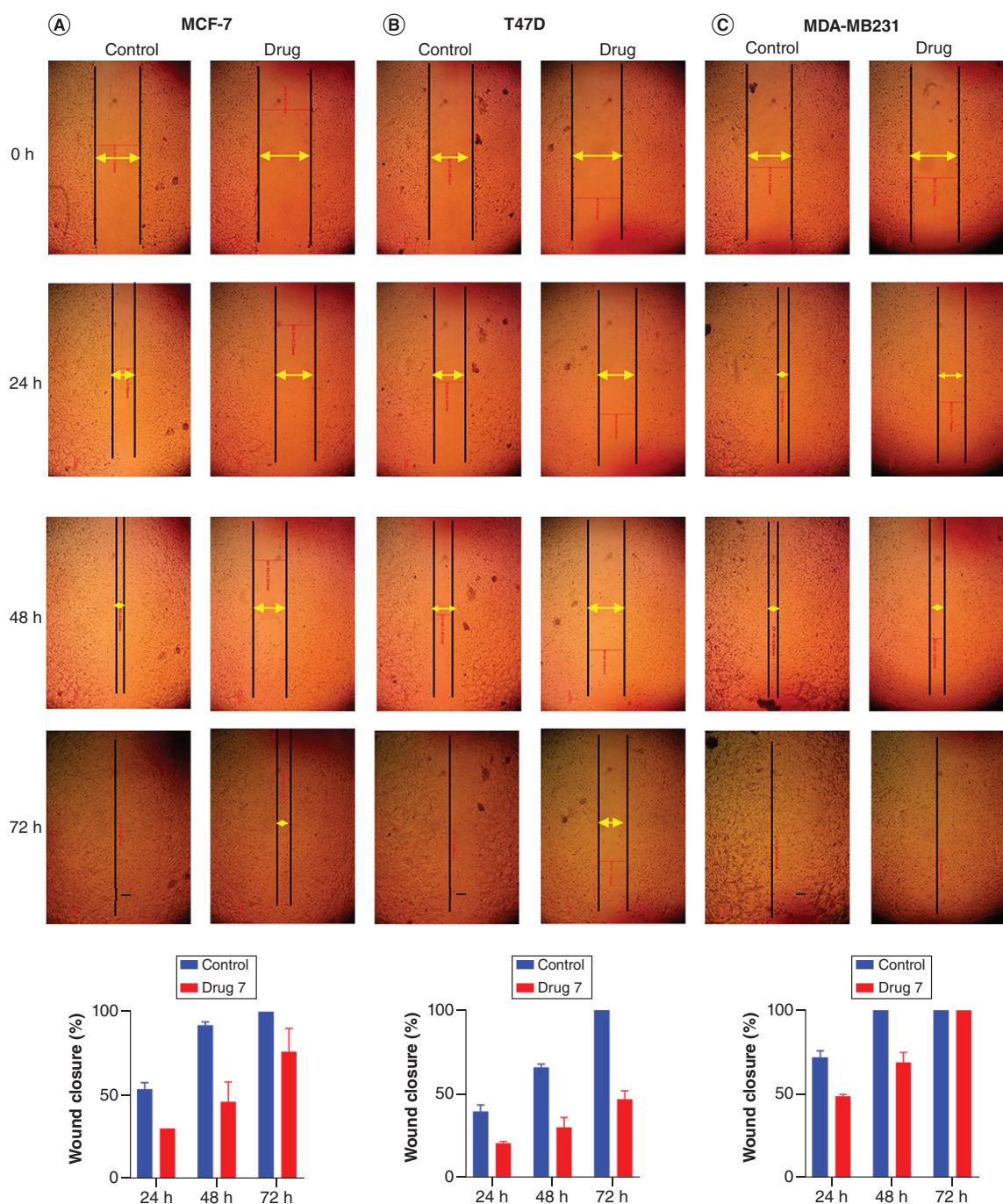


**Figure 8.** Effect of compound 7 on cell migration in MCF-7, T47D and MDA-MB231 cell lines. Images show the wound healing progress among the three cell lines at 0, 24, 48 and 72 h. The double-headed yellow arrows define the wound areas that take cells. Wound closure percentages for three cell lines are shown in the bar chart. As shown, compound 7 decreased cell migration in the three cell lines. (A) MCF-7. (B) T47d. (C) MDA-MB231.

showed that carbonic anhydrase inhibition interferes with the G1 phase during cell cycle progression. Furthermore, compound 7 induced an apoptotic effect against MCF-7, T47D and MDA-MB231 cell lines; the apoptotic effect on these breast cancer cell lines may be due to disruption in the pH of the cells, which is linked to carbonic anhydrase inhibition, leading to acidosis [86–88]. Apart from apoptosis, compound 7 also potently increased the level of autophagic cell death in MCF-7, T47D and MDA-MB231 cell lines. It has been reported that cells treated with carbonic anhydrase inhibitors showed an increase in the level of autophagy mediators (LC3, Beclin) [86,89] and hence

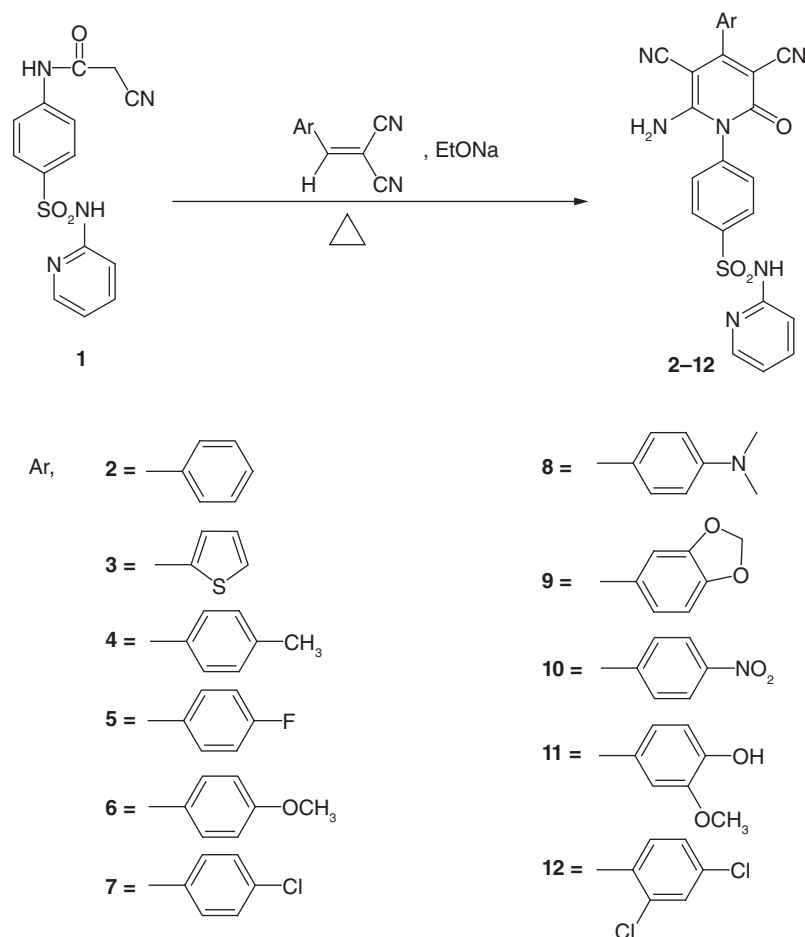


Figure 9. Synthetic route for compounds 2–12.

autophagy induction. Additionally, compound 7 showed an antimigratory effect on MCF-7 and MDA-MB231 cells and especially on the T47D cell line. Invasion and migration inhibition in cancer cells signifies a therapeutic strategy. Carbonic anhydrase inhibitors have previously been assessed as effective moieties in postponing cell migration [90]. In line with the previous research, compound 7 exerted an antimigratory effect, as evidenced by the wound healing assay. Compound 7 showed good results against cancer cell lines and also proved to be an effective CA IX inhibitor. Therefore compound 7 could be considered as a promising lead that could be further optimized as a CA IX inhibitor.

## Conclusion

In the present study, we investigated the potential use of novel pyridine–sulfonamide hybrids as potential anticancer agents, with a special emphasis on breast cancer. Compounds 2–12 were designed, synthesized and biologically tested for their anticancer activity. Among the 12 tested compounds, compounds 3, 5, 7 and 11 showed certain cytotoxic activities, with  $IC_{50}$  values ranging from 12.15 to 99.95  $\mu$ M, with the para chloro-derivative 7 showing the highest cytotoxic activity on the tested breast cancer cell lines. Moreover, compound 7 showed considerable induction of apoptosis and autophagy in all tested cell lines, as well as producing an observable delay in breast cancer cells' migration. Compound 7 exhibited CA IX inhibitory activity with an  $IC_{50}$  of  $253 \pm 12$  nM. These findings suggest that compound 7, which belongs to the sulfonamide–pyridine series, could be used as a potential therapeutic agent for breast cancer. Additional studies are needed to further define the anticancer activity of compound 7 *in vivo*.

## Summary points

- Breast cancer is considered one of the most challenging cancers to cure, due to drug resistance as well as metastasis.
- There are continuous efforts by medicinal chemistry researchers to discover novel anticancer agents with targeted mechanisms.
- Herein, molecular hybridization was used for the design of target compounds including both sulfonamide and pyridine scaffolds.
- Synthesis of 11 novel compounds was done through a one-pot synthetic procedure.
- Biological assays were performed, including cytotoxicity assays on three breast cancer cell lines
- Compound **7** showed the most potent activity against the three used cell lines.
- Compound **7** was subjected to further studies, including cell cycle analysis, apoptosis assessment, autophagy assay and wound healing assessment.
- Compound **7** exhibited carbonic anhydrase IX inhibition activity, with an  $IC_{50}$  of  $253 \pm 12$  nM.
- Molecular modeling through docking studies was done to explore the binding pattern between compound **7** and carbonic anhydrase IX.

## Supplementary data

To view the supplementary data that accompany this paper please visit the journal website at: [www.future-science.com/doi/suppl/10.4155/fmc-2022-0197](http://www.future-science.com/doi/suppl/10.4155/fmc-2022-0197)

## Financial &amp; competing interests disclosure

The authors have no relevant affiliations or financial involvement with any organization or entity with a financial interest in or financial conflict with the subject matter or materials discussed in the manuscript. This includes employment, consultancies, honoraria, stock ownership or options, expert testimony, grants or patents received or pending, or royalties.

No writing assistance was utilized in the production of this manuscript.

## References

Papers of special note have been highlighted as: • of interest; •• of considerable interest

1. Rashid HU, Xu YM, Muhammad Y, Wang LS, Jiang J. Research advances on anticancer activities of matrine and its derivatives: an updated overview. *Eur. J. Med. Chem.* 161, 205–238 (2019).
2. Ahmadi R, Ebrahimpzadeh MA. Resveratrol – a comprehensive review of recent advances in anticancer drug design and development. *Eur. J. Med. Chem.* 200, 112356 (2020).
- **Highlights the major important advances in the field of drug discovery for anticancer agents.**
3. Liang T, Sun X, Li W, Hou G, Gao F. 1,2,3-Triazole-containing compounds as anti-lung cancer agents: current developments, mechanisms of action, and structure–activity relationship. *Front. Pharmacol.* 12, 661173 (2021).
4. Jarak I, Varela CL, Da Silva ET, Roleira FFM, Veiga F, Figueiras A. Pluronic-based nanovehicles: recent advances in anticancer therapeutic applications. *Eur. J. Med. Chem.* 206, 112526 (2020).
5. Cui WQ, Aouidate A, Wang SG, Yu QLY, Li YH, Yuan SG. Discovering anti-cancer drugs via computational methods. *Front. Pharmacol.* 11, 733 (2020).
6. Anderson NM, Simon MC. The tumor microenvironment. *Curr. Biol.* 30(16), R921–R925 (2020).
7. Emami Nejad A, Najafgholian S, Rostami A *et al.* The role of hypoxia in the tumor microenvironment and development of cancer stem cell: a novel approach to developing treatment. *Cancer Cell Int.* 21(1), 62 (2021).
8. Gillies RJ, Brown JS, Anderson ARA, Gatenby RA. Eco-evolutionary causes and consequences of temporal changes in intratumoural blood flow. *Nat. Rev. Cancer* 18(9), 576–585 (2018).
9. Pastorekova S, Gillies RJ. The role of carbonic anhydrase IX in cancer development: links to hypoxia, acidosis, and beyond. *Cancer Metastasis Rev.* 38(1-2), 65–77 (2019).
10. Nejad AE, Najafgholian S, Rostami A *et al.* The role of hypoxia in the tumor microenvironment and development of cancer stem cell: a novel approach to developing treatment. *Cancer Cell Int.* 21(1), 62 (2021).
11. Shi R, Liao C, Zhang Q. Hypoxia-driven effects in cancer: characterization, mechanisms, and therapeutic implications. *Cells* 10(3), 678 (2021).
12. Ratcliffe PJ. Oxygen sensing and hypoxia signalling pathways in animals: the implications of physiology for cancer. *J. Physiol.* 591(8), 2027–2042 (2013).
13. Kim LC, Simon MC. Hypoxia-inducible factors in cancer. *Cancer Res.* 82(2), 195–196 (2022).

14. Guarnaccia L, Navone SE, Trombetta E *et al.* Angiogenesis in human brain tumors: screening of drug response through a patient-specific cell platform for personalized therapy. *Sci. Rep.* 8(1), 8748 (2018).
15. Ahn GO, Seita J, Hong BJ *et al.* Transcriptional activation of hypoxia-inducible factor-1 (HIF-1) in myeloid cells promotes angiogenesis through VEGF and S100A8. *Proc. Natl Acad. Sci. USA* 111(7), 2698–2703 (2014).
16. Pastorek J, Pastorekova S. Hypoxia-induced carbonic anhydrase IX as a target for cancer therapy: from biology to clinical use. *Semin. Cancer Biol.* 31, 52–64 (2015).
17. Pastorek J, Pastorekova S, Callebaut I *et al.* Cloning and characterization of MN, a human tumor-associated protein with a domain homologous to carbonic anhydrase and a putative helix-loop-helix DNA binding segment. *Oncogene* 9(10), 2877–2888 (1994).
18. Kumar S, Rulhania S, Jaswal S, Monga V. Recent advances in the medicinal chemistry of carbonic anhydrase inhibitors. *Eur. J. Med. Chem.* 209(1), 112923 (2021).
19. Parkkila S, Parkkila AK, Saarnio J *et al.* Expression of the membrane-associated carbonic anhydrase isozyme XII in the human kidney and renal tumors. *J. Histochem. Cytochem.* 48(12), 1601–1608 (2000).
20. Haapasalo J, Hilvo M, Nordfors K *et al.* Identification of an alternatively spliced isoform of carbonic anhydrase XII in diffusely infiltrating astrocytic gliomas. *Neuro Oncol.* 10(2), 131–138 (2008).
21. Korhonen K, Parkkila AK, Helen P *et al.* Carbonic anhydrases in meningiomas: association of endothelial carbonic anhydrase II with aggressive tumor features. *J. Neurosurg.* 111(3), 472–477 (2009).
22. Lou YM, McDonald PC, Oloumi A *et al.* Targeting tumor hypoxia: suppression of breast tumor growth and metastasis by novel carbonic anhydrase IX inhibitors. *Cancer Res.* 71(9), 3364–3376 (2011).
23. Sung H, Ferlay J, Siegel RL *et al.* Global cancer statistics 2020: GLOBOCAN estimates of incidence and mortality worldwide for 36 cancers in 185 countries. *CA Cancer J. Clin.* 71(3), 209–249 (2021).
24. Nguyen QH, Pervolarakis N, Blake K *et al.* Profiling human breast epithelial cells using single cell RNA sequencing identifies cell diversity. *Nat. Commun.* 9(1), 2028 (2018).
- **Properties of cancer cells and illustration of cell heterogeneity.**
25. Kogel D, Linder B, Brunschweiler A, Chines S, Behl C. At the crossroads of apoptosis and autophagy: multiple roles of the co-chaperone BAG3 in stress and therapy resistance of cancer. *Cells* 9(3), 574 (2020).
- **The role of apoptosis and autophagy in cancer cell death.**
26. Hanahan D, Weinberg RA. Hallmarks of cancer: the next generation. *Cell* 144(5), 646–674 (2011).
- **Very important review covering many interesting points related to our current work.**
27. King EK, Losier TT, Russell CR. Regulation of autophagy enzymes by nutrient signaling. *Trends Biochem. Sci.* 46(8), 687–700 (2021).
- **Highlights the importance of autophagy.**
28. Di Bartolomeo S, Latella L, Zarbalis K, Di Sano F. Editorial: autophagy in mammalian development and differentiation. *Front. Cell Dev. Biol.* 9, 722821 (2021).
29. Fang YY, Tan J, Zhang Q. Signaling pathways and mechanisms of hypoxia-induced autophagy in the animal cells. *Cell Biol. Int.* 39(8), 891–898 (2015).
30. Lim KH, Staudt LM. Toll-like receptor signaling. *Cold Spring Harb. Perspect. Biol.* 5(1), a011247 (2013).
31. Rosenfeldt MT, Ryan KM. The multiple roles of autophagy in cancer. *Carcinogenesis* 32(7), 955–963 (2011).
32. Ghorab MM, Heiba HI, Khalil AI, El Ella DaA, Noaman E. Computer-based ligand design and synthesis of some new sulfonamides bearing pyrrole or pyrrolopyrimidine moieties having potential antitumor and radioprotective activities. *Phosphorus Sulfur Rel. Elem.* 183(1), 90–104 (2008).
33. Muller-Schiffmann A, Marz-Berberich J, Andreyeva A *et al.* Combining independent drug classes into superior, synergistically acting hybrid molecules. *Angew. Chem. Int. Edit. Engl.* 49(46), 8743–8746 (2010).
34. Ghorab MM, El-Gazzar MG, Alsaïd MS. Synthesis and anti-breast cancer evaluation of novel N-(guanidinyl)benzenesulfonamides. *Int. J. Mol. Sci.* 15(4), 5582–5595 (2014).
- **Includes important chemical and biological details related to our study.**
35. Eldehna WM, Fares M, Ceruso M *et al.* Amido/ureidosubstituted benzenesulfonamides–isatin conjugates as low nanomolar/subnanomolar inhibitors of the tumor-associated carbonic anhydrase isoform XII. *Eur. J. Med. Chem.* 110, 259–266 (2016).
- **Important article relating to sulfonamides and carbonic anhydrase inhibition.**
36. Ghorab MM, Alsaïd MS, Al-Ansary GH, Abdel-Latif GA, Abou El Ella DA. Analogue based drug design, synthesis, molecular docking and anticancer evaluation of novel chromene sulfonamide hybrids as aromatase inhibitors and apoptosis enhancers. *Eur. J. Med. Chem.* 124, 946–958 (2016).
37. Eldehna WM, Abo-Ashour MF, Nocentini A *et al.* Novel 4/3-((4-oxo-5-(2-oxoindolin-3-ylidene)thiazolidin-2-ylidene) amino) benzenesulfonamides: synthesis, carbonic anhydrase inhibitory activity, anticancer activity and molecular modelling studies. *Eur. J. Med. Chem.* 139, 250–262 (2017).

38. Karali N, Akdemir A, Goktas F *et al.* Novel sulfonamide-containing 2-indolinones that selectively inhibit tumor-associated alpha carbonic anhydrases. *Bioorg. Med. Chem.* 25(14), 3714–3718 (2017).
39. Supuran CT. Advances in structure-based drug discovery of carbonic anhydrase inhibitors. *Expert Opin. Drug Discov.* 12(1), 61–88 (2017).
40. Eldehna WM, Nocentini A, Al-Rashood ST *et al.* Tumor-associated carbonic anhydrase isoform IX and XII inhibitory properties of certain isatin-bearing sulfonamides endowed with *in vitro* antitumor activity towards colon cancer. *Bioorg. Chem.* 81, 425–432 (2018).
41. Gul HI, Yamali C, Sakagami H *et al.* New anticancer drug candidates sulfonamides as selective hCA IX or hCA XII inhibitors. *Bioorg. Chem.* 77, 411–419 (2018).
42. Nocentini A, Trallori E, Singh S *et al.* 4-Hydroxy-3-nitro-5-ureido-benzenesulfonamides selectively target the tumor-associated carbonic anhydrase isoforms IX and XII showing hypoxia-enhanced antiproliferative profiles. *J. Med. Chem.* 61(23), 10860–10874 (2018).
43. Peerzada MN, Khan P, Ahmad K, Hassan MI, Azam A. Synthesis, characterization and biological evaluation of tertiary sulfonamide derivatives of pyridyl–indole based heteroaryl chalcone as potential carbonic anhydrase IX inhibitors and anticancer agents. *Eur. J. Med. Chem.* 155, 13–23 (2018).
44. Cecchi A, Winum JY, Innocenti A *et al.* Carbonic anhydrase inhibitors: synthesis and inhibition of cytosolic/tumor-associated carbonic anhydrase isozymes I, II, and IX with sulfonamides derived from 4-isothiocyanato-benzolamide. *Bioorg. Med. Chem. Lett.* 14(23), 5775–5780 (2004).
45. Garaj V, Puccetti L, Fasolis G *et al.* Carbonic anhydrase inhibitors: synthesis and inhibition of cytosolic/tumor-associated carbonic anhydrase isozymes I, II, and IX with sulfonamides incorporating 1,2,4-triazine moieties. *Bioorg. Med. Chem. Lett.* 14(21), 5427–5433 (2004).
46. Aday B, Ulus R, Tanc M, Kaya M, Supuran CT. Synthesis of novel 5-amino-1,3,4-thiadiazole-2-sulfonamide containing acridine sulfonamide/carboxamide compounds and investigation of their inhibition effects on human carbonic anhydrase I, II, IV and VII. *Bioorg. Chem.* 77, 101–105 (2018).
47. Koch G. Medicinal chemistry: editorial. *CHIMIA* 71(10), 643 (2017).
48. McDonald PC, Chia S, Bedard PL *et al.* A phase I study of SLC-0111, a novel inhibitor of carbonic anhydrase IX, in patients with advanced solid tumors. *Am. J. Clin. Oncol.* 43(7), 484–490 (2020).
49. Gieling RG, Babur M, Mamnani L *et al.* Antimetastatic effect of sulfamate carbonic anhydrase IX inhibitors in breast carcinoma xenografts. *J. Med. Chem.* 55(11), 5591–5600 (2012).
50. Williams KJ, Gieling RG. Preclinical evaluation of ureidosulfamate carbonic anhydrase IX/XII inhibitors in the treatment of cancers. *Int. J. Mol. Sci.* 20(23), 6080 (2019).
51. Mboge MY, Mahon BP, Lamas N *et al.* Structure activity study of carbonic anhydrase IX: selective inhibition with ureido-substituted benzenesulfonamides. *Eur. J. Med. Chem.* 132, 184–191 (2017).
52. Mboge MY, Chen Z, Wolff A *et al.* Selective inhibition of carbonic anhydrase IX over carbonic anhydrase XII in breast cancer cells using benzene sulfonamides: disconnect between activity and growth inhibition. *PLOS ONE* 13(11), e0207417 (2018).
53. Bailón-Moscoso N, Romero-Benavides JC, Ostrosky-Wegman P. Development of anticancer drugs based on the hallmarks of tumor cells. *Tumour Biol.* 35(5), 3981–3995 (2014).
54. Lovitt CJ, Shelper TB, Avery VM. Doxorubicin resistance in breast cancer cells is mediated by extracellular matrix proteins. *BMC Cancer* 18(1), 41 (2018).
55. Viegas Junior C, Danuello A, Bolzani V, Barreiro E, Fraga C. Molecular hybridization: a useful tool in the design of new drug prototypes. *Curr. Med. Chem.* 14, 1829–1852 (2007).
56. Narendar P, Parthiban J, Anbalagan N, Gunasekaran V, Thomas Leonard J. Pharmacological evaluation of some new 2-substituted pyridine derivatives. *Biol. Pharm. Bull.* 26(2), 182–187 (2003).
57. Menegatti R, Silva GMS, Zapata-Sudo G *et al.* Design, synthesis, and pharmacological evaluation of new neuroactive pyrazolo[3,4-b]pyrrolo[3,4-d]pyridine derivatives with *in vivo* hypnotic and analgesic profile. *Bioorg. Med. Chem.* 14(3), 632–640 (2006).
58. El-Naggar M, Almahli H, Ibrahim HS, Eldehna WM, Abdel-Aziz HA. Pyridine-ureas as potential anticancer agents: synthesis and *in vitro* biological evaluation. *Molecules* 23(6), 1459 (2018).
59. Albratty M, Alhazmi HA. Novel pyridine and pyrimidine derivatives as promising anticancer agents: a review. *Arabian J. Chem.* 15(6), 103846 (2022).
60. Krasavin M, Kalinin S, Sharonova T, Supuran CT. Inhibitory activity against carbonic anhydrase IX and XII as a candidate selection criterion in the development of new anticancer agents. *J. Enzyme Inhib. Med. Chem.* 35(1), 1555–1561 (2020).
61. Deka S, Mohan S, Saravanan J *et al.* Syntheses, characterization and in-vitro anti-inflammatory activity of some novel thiophenes. *Maced. J. Med. Sci.* 5, 159–163 (2012).
62. Ragab FA, Heiba HI, El-Gazzar MG, Abou-Seri SM, El-Sabbagh WA, El-Hazek RM. Synthesis of novel thiadiazole derivatives as selective COX-2 inhibitors. *Med. Chem. Commun.* 7(12), 2309–2327 (2016).
63. Berman HM, Westbrook J, Feng Z *et al.* The Protein Data Bank. *Nucleic Acids Res.* 28(1), 235–242 (2000).

64. Zakšauskas A, Čapkauskaitė E, Paketurytė-Latvė V *et al.* Methyl 2-halo-4-substituted-5-sulfamoyl-benzoates as high affinity and selective inhibitors of carbonic anhydrase IX. *Int. J. Mol. Sci.* 23(1), 130 (2022).
65. Morris GM, Huey R, Lindstrom W *et al.* AutoDock4 and AutoDockTools4: automated docking with selective receptor flexibility. *J. Comput. Chem.* 30(16), 2785–2791 (2009).
66. Santos-Martins D, Forli S, Ramos MJ, Olson AJ. AutoDock4(Zn): an improved AutoDock force field for small-molecule docking to zinc metalloproteins. *J. Chem. Inf. Model.* 54(8), 2371–2379 (2014).
67. O'boyle NM, Banck M, James CA, Morley C, Vandermeersch T, Hutchison GR. Open Babel: an open chemical toolbox. *J. Cheminform.* 3, 33 (2011).
68. Halgren TA. MMFF VI. MMFF94s option for energy minimization studies. *J. Comput. Chem.* 20(7), 720–729 (1999).
69. Trott O, Olson AJ. AutoDock Vina: improving the speed and accuracy of docking with a new scoring function, efficient optimization, and multithreading. *J. Comput. Chem.* 31(2), 455–461 (2010).
70. Pettersen EF, Goddard TD, Huang CC *et al.* UCSF Chimera – a visualization system for exploratory research and analysis. *J. Comput. Chem.* 25(13), 1605–1612 (2004).
71. Jacobs GP. A review of the effects of gamma radiation on pharmaceutical materials. *J. Biomater. Appl.* 10(1), 59–96 (1995).
72. El-Gaby MSA, Abdel-Gawad SM, Ghorab MM, Heiba HI, Aly HM. Synthesis and biological activity of some novel thieno[2,3-b]quinoline, quinolino[3',2':4,5] thieno[3,2-d]pyrimidine and pyrido[2',3':4,5] thieno[2,3-b]quinoline derivatives. *Phosphorus Sulfur Silicon Relat. Elem.* 181(2), 279–297 (2006).
73. Singh BK, Parwate DV, Das Sarma IB, Shukla SK. Study on gamma and electron beam sterilization of third generation cephalosporins cefdinir and cefixime in solid state. *Radiat. Phys. Chem.* 79(10), 1079–1087 (2010).
74. Crucq A-S, Deridder V, Tilquin B. Radiostability of pharmaceuticals under different irradiation conditions. *Radiat. Phys. Chem.* 72(2), 355–361 (2005).
75. Zalewski P, Skibiński R, Szymanowska-Powalowska D, Piotrowska H, Bednarski W, Cielecka-Piontek J. Radiolytic studies of cefozopran hydrochloride in the solid state. *Electron. J. Biotechnol.* 25, 28–32 (2017).
76. Huey R, Morris GM, Olson AJ, Goodsell DS. A semiempirical free energy force field with charge-based desolvation. *J. Comput. Chem.* 28(6), 1145–1152 (2007).
77. Bell EW, Zhang Y. DockRMSD: an open-source tool for atom mapping and RMSD calculation of symmetric molecules through graph isomorphism. *J. Cheminform.* 11(1), 40 (2019).
78. Skehan P, Storeng R, Scudiero D *et al.* New colorimetric cytotoxicity assay for anticancer-drug screening. *J. Natl Cancer Inst.* 82(13), 1107–1112 (1990).
79. Darzynkiewicz Z, Bedner E, Smolewski P. Flow cytometry in analysis of cell cycle and apoptosis. *Semin. Hematol.* 38(2), 179–193 (2001).
80. Fathy U, Abd El Salam HA, Fayed EA, Elgamil AM, Gouda A. Facile synthesis and *in vitro* anticancer evaluation of a new series of tetrahydroquinoline. *Heliyon* 7(10), e08117 (2021).
81. Bashmail HA, Alamoudi AA, Noorwali A, Hegazy GA, Ajabnoor GM, Al-Abd AM. Thymoquinone enhances paclitaxel anti-breast cancer activity via inhibiting tumor-associated stem cells despite apparent mathematical antagonism. *Molecules* 25(2), 426 (2020).
82. Yousefi S, Simon HU. Autophagy in cancer and chemotherapy. *Results Probl. Cell Differ.* 49, 183–190 (2009).
83. Zeng F, Ju RJ, Liu L, Xie HJ, Mu LM, Lu WL. Efficacy in treating lung metastasis of invasive breast cancer with functional vincristine plus dasatinib liposomes. *Pharmacology* 101(1-2), 43–53 (2018).
84. Supuran CT. Indisulam: an anticancer sulfonamide in clinical development. *Expert Opin. Investig. Drugs* 12(2), 283–287 (2003).
85. Ruzzolini J, Laurenzana A, Andreucci E *et al.* A potentiated cooperation of carbonic anhydrase IX and histone deacetylase inhibitors against cancer. *J. Enzyme Inhib. Med. Chem.* 35(1), 391–397 (2020).
86. Temiz E, Koyuncu I, Durgun M *et al.* Inhibition of carbonic anhydrase IX promotes apoptosis through intracellular pH level alterations in cervical cancer cells. *Int. J. Mol. Sci.* 22(11), 6098 (2021).
87. Cianchi F, Vinci MC, Supuran CT *et al.* Selective inhibition of carbonic anhydrase IX decreases cell proliferation and induces ceramide-mediated apoptosis in human cancer cells. *J. Pharmacol. Exp. Ther.* 334(3), 710–719 (2010).
88. Koyuncu I, Gonel A, Kocyigit A, Temiz E, Durgun M, Supuran CT. Selective inhibition of carbonic anhydrase-IX by sulphonamide derivatives induces pH and reactive oxygen species-mediated apoptosis in cervical cancer HeLa cells. *J. Enzyme Inhib. Med. Chem.* 33(1), 1137–1149 (2018).
89. Mohammadpour R, Safarian S, Ejeian F, Sheikholya-Lavasani Z, Abdolmohammadi MH, Sheinabi N. Acetazolamide triggers death inducing autophagy in T-47D breast cancer cells. *Cell Biol. Int.* 38(2), 228–238 (2014).
90. Ward C, Meehan J, Mullen P *et al.* Evaluation of carbonic anhydrase IX as a therapeutic target for inhibition of breast cancer invasion and metastasis using a series of *in vitro* breast cancer models. *Oncotarget* 6(28), 24856–24870 (2015).